



Article

The Removal of As(III) Using a Natural Laterite Fixed-Bed Column Intercalated with Activated Carbon: Solving the Clogging Problem to Achieve Better Performance

Régie Dimanche Ouedraogo, Corneille Bakouan, Abdoul Karim Sakira, Brahim Sorgho, Boubié Guel, Touridomon Issa Somé, Anne-Lise Hantson, Eric Ziemons, Dominique Mertens, Philippe Hubert et al.

Special Issue


Development and Applications of Porous Materials in Adsorptions

Edited by
Dr. Byong Chol Bai



Article

The Removal of As(III) Using a Natural Laterite Fixed-Bed Column Intercalated with Activated Carbon: Solving the Clogging Problem to Achieve Better Performance

Régie Dimanche Ouedraogo ¹, Corneille Bakouan ^{1,2,3} , Abdoul Karim Sakira ^{4,5}, Brahima Sorgho ¹, Boubié Guel ^{1,*} , Touridomon Issa Somé ⁴, Anne-Lise Hantson ³, Eric Ziemons ⁶ , Dominique Mertens ⁵, Philippe Hubert ⁶ and Jean-Michel Kauffmann ⁵

- ¹ Laboratoire de Chimie Moléculaire et des Matériaux (LC2M)/Equipe Chimie Physique et d'Electrochimie, U.F.R-SEA, Université Joseph KI-ZERBO, 03 BP 7021, Ouagadougou 03, Burkina Faso; ouedraogoregie@gmail.com (R.D.O.); bakouancorneille@gmail.com (C.B.); sobrah20@yahoo.fr (B.S.)
- ² Laboratoire de Recherche et Développement (LRD), Unité de Formation en Sciences et Technologies (UFR-ST), Université de Ouahigouya, 01 BP 346, Ouahigouya 01, Burkina Faso
- ³ Département Génie des Procédés Chimiques et Biochimiques, Faculté Polytechnique, UMONS, Place du Parc 21, 7000 Mons, Belgium; anne-lise.hantson@umons.ac.be
- ⁴ Laboratoire de Chimie Analytique et de Toxicologie, Laboratoire de Toxicologie, Environnement et Santé, U.F.R-SDS, Université Joseph KI-ZERBO, 03 BP 7021, Ouagadougou 03, Burkina Faso; karim_sakira@yahoo.fr (A.K.S.); tsome66@gmail.com (T.I.S.)
- ⁵ Laboratoire de Chimie Analytique Instrumentale et Bioélectrochimie, Université Libre de Bruxelles (ULB), Campus de la Plaine, CP 205/6, 1050 Bruxelles, Belgium; dmertens@ulb.ac.be (D.M.); jmkauf@ulb.ac.be (J.-M.K.)
- ⁶ Laboratoire de Chimie Analytique Pharmaceutique, VibraSante Hub, Département de Pharmacie, Université de Liège (ULiège), Avenue Hippocrate 15, B36, 4000 Liège, Belgium; eziemons@uliege.be (E.Z.); ph.hubert@liege.be (P.H.)
- * Correspondence: boubie.guel@ujkz.bf or boubieguel@yahoo.fr; Tel.: +226-68-51-50-44 or +226-76-64-54-69



Citation: Ouedraogo, R.D.; Bakouan, C.; Sakira, A.K.; Sorgho, B.; Guel, B.; Somé, T.I.; Hantson, A.-L.; Ziemons, E.; Mertens, D.; Hubert, P.; et al. The Removal of As(III) Using a Natural Laterite Fixed-Bed Column Intercalated with Activated Carbon: Solving the Clogging Problem to Achieve Better Performance. *Separations* **2024**, *11*, 129. <https://doi.org/10.3390/separations11040129>

Academic Editor: Byong Chol Bai

Received: 26 March 2024

Revised: 15 April 2024

Accepted: 17 April 2024

Published: 22 April 2024



Copyright: © 2024 by the authors. Licensee MDPI, Basel, Switzerland. This article is an open access article distributed under the terms and conditions of the Creative Commons Attribution (CC BY) license (<https://creativecommons.org/licenses/by/4.0/>).

Abstract: Natural laterite fixed-bed columns intercalated with two types of layers (inert materials, such as fine sand and gravel, and adsorbent materials, such as activated carbon prepared from *Balanites aegyptiaca* (BA-AC)) were used for As(III) removal from an aqueous solution. Investigations were carried out to solve the problem of column clogging, which appears during the percolation of water through a natural laterite fixed-bed column. Experimental tests were conducted to evaluate the hydraulic conductivities of several fixed-bed column configurations and the effects of various parameters, such as the grain size, bed height, and initial As(III) concentration. The permeability data show that, among the different types of fixed-bed columns investigated, the one filled with repeating layers of laterite and activated carbon is more suitable for As(III) adsorption, in terms of performance and cost, than the others (i.e., non-intercalated laterite; non-intercalated activated carbon, repeating layers of laterite and fine sand; and repeating layers of laterite and gravel). A study was carried out to determine the most efficient column using breakthrough curves. The breakthrough increased from 15 to 85 h with an increase in the bed height from 20 to 40 cm and decreased from 247 to 32 h with an increase in the initial As(III) concentration from 0.5 to 2 mg/L. The Bohart–Adams model results show that increasing the bed height induced a decrease in the k_{AB} and N_0 values. The critical bed depths determined using the bed depth service time (BDST) model for As(III) removal were 15.23 and 7.98 cm for 1 and 20% breakthroughs, respectively. The results show that the new low-cost adsorptive porous system based on laterite layers with alternating BA-AC layers can be used for the treatment of arsenic-contaminated water.

Keywords: laterite; balanites aegyptiaca; percolation; activated carbon; hydraulic conductivity

1. Introduction

Environmental pollution is a major concern. It has been reported that pollutants are generally introduced into the environment as a result of anthropogenic activities. Among them, heavy metals, such as Cd, Cu, Hg, Ni, Zn, and Pb, are known to be toxic to living organisms and to present high potential risks to human health due to their accumulation in the food chain due to anthropogenic activities [1,2]. Alongside these pollutants, arsenic (As) contamination in groundwater has recently become a global issue [2–5]. In Burkina Faso, it was reported that the groundwaters in several localities were polluted with arsenic, whose concentrations in pit and drilling waters are extremely high compared to the World Health Organization's (WHO) standard value (0.01 mg/L) [6]. Arsenic is present in groundwater as arsenite (As(III)) and arsenate (As(V)), according to the redox conditions [7–9]. Owing to its toxic effects and in the context of water shortages in developing countries, it is urgent to develop a simple and suitable methodology for the removal of arsenic from contaminated groundwaters. The most current approaches for arsenic removal include precipitation, coagulation by adding lime or coagulants to water, separation using membranes, an ion exchange process, adsorption, ultrafiltration, reverse osmosis, ozone oxidation, bioremediation, and electrochemical treatment [10–17]. Among all of these approaches, adsorption has been proven to be the most promising method because of its high efficiency, ease of handling, and the availability of several types of adsorbent materials. Among these adsorbents, natural laterites have been the subject of many investigations since they were shown to have potential applications in arsenic removal from groundwater [18–24]. In our context, natural laterites are widely available in the country and can be used for low-cost arsenic removal. Indeed, many studies have documented arsenic removal by adsorption on natural laterite using the batch mode, as well as fixed-bed column systems [18–24]. In an effort to develop an efficient, low-cost, and easily applied method, our previous research focused on As(III) adsorption in the batch mode using local natural laterites [21,22]. In the batch mode, we achieved an elimination rate of 97.30% for As(III) at a dose of 0.75 g of laterite [22]. The adsorption capacity was 0.30 mg/g [22]. These investigations paved the way for the first uses of local natural laterites from Burkina Faso for As(III) remediation from drinking water using fixed-bed columns. Indeed, the fixed-bed system provides greater flexibility compared to the batch mode. One of the advantages of the fixed-bed system is the prediction of the breakthrough curve, which determines the functional longevity of the adsorbent beds and regeneration time. Although fixed-bed systems possess several advantages, they may be subject to permeability issues due to the percolator material. This is the case for laterite soils, which are known to have low permeability to water when used as percolator materials in fixed-bed systems [25]. It was reported that, because of laterites' low permeability, supporting material may be required for its use in columns [25]. It is worth noting that there is little published information on the hydraulic conductivity of laterite soils in Western Africa [26]. After carrying out an exhaustive literature review, we noted that the percolation treatment process for arsenic adsorption using fixed-bed column percolation has been improved upon by several authors, who proposed various column configurations that combine laterite layers and adsorbent/inert materials to solve shortcomings in the operation of the system [12,18,20,23,24]. Even though the column designs are different, the most current approach consists of one or two laterite layers integrated in a column configuration of successive layers of inert and/or adsorbent materials [12,18,20,23]. A lot of studies have addressed the fixed-bed column adsorption of As(III) on laterite soil [12,19,20,23,24]. The technical details of these configurations are given in (Supplementary Information (SI1)). However, it must be noted that in all of the above studies, no further tests were carried out using fixed-bed columns with small-sized particles of laterite, and no permeability data were provided to explain why these configurations improved the performance of the percolation treatment.

Our team also investigated arsenic removal using a fixed-bed field column filled only with local natural laterites from Burkina Faso. We showed that a better adsorption capacity during the column percolation process could only be achieved with larger diameters and greater

heights of the bed and smaller adsorbent pore sizes [21] (Supplementary Information (SI2)). As a result, we increased the fixed-bed field column's diameter and varied the laterite particles' sizes [21] (Supplementary Information (SI2)). However, contrary to previous results in the literature, our investigations show that fixed-bed column systems for use in arsenic removal encounter several shortcomings, particularly the clogging of the column with small lateritic particles, which can cause the flow of water through the column to slow down in the long run [21] (Supplementary Information (SI2)). Clogging is generally defined as a process that causes a reduction in the performance of an adsorbent due to the deposition of suspended or dissolved materials on its outer surface or within the pores [27–29]. Clogging can be related to different modes, such as cake formation and pore blockage by fine particles [30]. It has been reported that nanomaterials, which exist as small particles in a fine powder form, cause hydraulic problems by clogging column-based filters [24].

Developing an understanding of the clogging process that occurs during arsenic solution percolation constitutes the key element of our study. To the best of our knowledge, our study is the first in-depth study that has been conducted to understand the issue of clogging that occurs during solution percolation through a fixed-bed field column filled only with local natural laterites. As demonstrated in the literature, an artificial support material is needed to improve the permeability of the laterite soil in the fixed-bed column. In the present work, we adopted a different approach to that already reported in the literature. Our approach is based on a method using alternating layers in which the fixed-bed column is filled with repeating intercalated layers of laterite and inert/adsorbent materials. These layers are repeated several times for the almost complete removal of arsenic. The arsenic concentration in the water passing through this kind of column is very low if the water is allowed to pass through it very slowly. However, if the passing rate increases, the removal efficiency is reduced significantly. The layer to be intercalated between the laterite layers could be either an inert material (fine sand, coarse sand, or gravel) or an adsorbent material that also adsorbs very well without having negative impacts on the targeted pollutant. Among the several adsorbents currently in use, activated carbon seems more suitable because of its high adsorption capacity, which is due to its large specific surface area and the presence of surface charges induced by its chemical composition [31–33]. The use of available waste as raw material to prepare activated carbon appears to be a good alternative to achieve a low-cost pollutant removal process [32–34]. We carried out our investigations by first choosing the two inert materials (fine sand and gravel) and an adsorbent material, which was activated carbon prepared from available raw materials (*Balanites aegyptiaca* (BA) cores). The present investigations are the first ones to be directed toward developing an understanding of the factors that control the problem of clogging during As(III) removal in a laterite fixed-bed field column, with an aim of gaining insights into the rational design of a new low-cost adsorptive porous system based on laterite layers alternated with three types of layers: activated carbon, fine sand, and gravel. Our investigations establish which column configurations are likely to overcome the problem of clogging that occurs when an As(III) solution percolates in a fixed-bed column.

This study aims to address the issue of column clogging that occurs during water percolation through a large field fixed-bed column containing natural laterite by designing a simple, reliable, and low-energy treatment system for arsenic-contaminated water. We conducted experimental tests to compare the hydraulic conductivities of three laterite fixed-bed column configurations. The first column was intercalated with an adsorbent material (activated carbon derived from *Balanites aegyptiaca* (BA-AC)); the second and third were intercalated with fine sand and gravel, respectively, as the inert materials. For the most efficient system, we investigated the influence of various parameters, including the grain size of the laterite particles, column bed height, and initial concentration of As(III), correlating the experimental data with a dynamic model (BDST approach) to predict the overall adsorption behavior.

2. Materials and Methods

2.1. Materials

The laterite and sand samples used in this study were collected in the localities of Dano and Bobo-Dioulasso, in the southwestern and southern regions of Burkina Faso, respectively, at the following coordinates: 11°07'36.1" N and 3°02'39.5" W; 12°20'36.96" N and 3°41'27.276" W. The samples were designated as DA laterite and BD sand, respectively.

The cores of *Balanites aegyptiaca*, which were used as the raw material, were collected from Balanites trees located in Ouagadougou, the capital of the country. These cores were washed with plenty of water and then dried in the sun for 5 d. They were crushed using a rotary jaw crusher to hold the hull. The latter was ground using a mortar and then sieved to retain particles with sizes ranging between 1.0 and 1.5 mm.

2.2. Chemicals

All solutions used in this study were prepared with ultrapure water with a resistivity of 18.2 MΩ.cm. The material used to prepare the different solutions was soaked in nitric acid (5%) for at least 12 h and rinsed with ultrapure water before use. The stock solution of As(III) was prepared from NaAsO₂ (99%, Merck, Rahway, NJ, USA). All reagents from Prolabo (HNO₃ 65%, NaOH, HCl 37%, and H₃PO₄ 85%) were of analytical grade.

The 1000 mg/L arsenic (III) stock solution was prepared by dissolving an appropriate mass of NaAsO₂ (99%, Merck Ltd., Rahway, NJ, USA) in a 1 L volume of milli-Q water. All working solutions, which had concentrations of 0.5, 1, and 2 mg/L, were obtained by diluting the stock solution.

2.3. Experimental Methods

2.3.1. Characterization of Adsorbent Materials

Physical and Chemical Properties of Laterite Sample

The characterization of the laterite sample, named DA laterite, was described in our previous study [22]. Elementary chemical analysis was performed by ICP (ICP-AES-IRIS Intrepid II XSP model). An amount of 0.25 g of laterite samples was digested in a microwave oven in 4 mL of HF (30% w/w), 3 mL of H₂SO₄ (96% w/w), and 3 mL of HNO₃ (65% w/w).

The specific surface area and pore volume of the laterite samples were determined by a BET analysis using a BelSorp-max instrument run with the Bel Japan Inc. software (Midori, Sumida, Tokyo, Japan). The samples were degassed and dehydrated for 24 h at 200 °C under a vacuum. The method used is based on the nitrogen adsorption/desorption isotherms at 77 K.

X-ray powder diffraction (XRPD) was carried out using a D8 Advance Davinci Bruker X-ray generator diffractometer (working at a 40 mA generator current and a 40 kV generator voltage with Cu-Kα radiation ($\lambda = 1.54060 \text{ \AA}$)). The XRPD data were recorded at a scanning speed of 0.02° s⁻¹ and at 2θ angles with values ranging from 5° to 70°.

Using KBr pellets containing 2% in weight of natural laterite powders (or laterites residues), the FTIR spectra were collected between 400 and 4000 cm⁻¹ in the transmission mode at a 4 cm⁻¹ resolution on Shimadzu FTIR-8400S equipment.

We showed that the laterite sample contains major phases, such as quartz (SiO₂), kaolinite (Al₂Si₂O₅(OH)₄), hematite (Fe₂O₃), and goethite (FeO(OH)) [22]. The physical properties of DA laterite are shown in Table 1, and its chemical composition is presented in Table 2 [22].

Table 1. Properties of DA laterite [22].

Properties	
pH _{PZC}	4.75
Bulk density (g/cm ³)	2.40
Anion exchange capacity (cmol·kg ⁻¹)	194.74
BET surface area (m ² /g)	35.08

Table 2. Chemical composition of DA laterite [22].

Chemical Composition (%)	
Fe ₂ O ₃	20.40
Al ₂ O ₃	19.10
SiO ₂	45.00
K ₂ O	0.36
Na ₂ O	0.20
TiO ₂	1.40
MgO, MnO ₂ , BaO, CaO	Traces

Two samples of laterite with grain sizes ranging between $0.900 \leq G_1 < 1.250$ mm and $0.425 \leq G_2 < 0.900$ mm were used to investigate the influence of the grain size on column clogging.

The free swelling index is an important characteristic in this study because it permits the qualitative characterization of the swelling of laterite. It was determined using a standard test. Masses (m) of 163 g, 290 g, and 439 g of dried laterite were placed in graduated test tubes. A quantity of distilled water was added, and the whole mixture was shaken regularly for one minute to suspend the laterite. The measurement of the height of the deposit was carried out as a function of time.

The swelling index was calculated using Equation (1):

$$I_g = \left[\left(V_f - V_i \right) / V_i \right] \times 100 \quad (1)$$

where I_g is the swelling index, and V_i and V_f are the initial and final volumes of DA, respectively.

Preparation and Characterization of Activated Carbon

Preparation of the activated carbon

The cores of the *Balanites aegyptiaca* kernels, which were used as precursors, were impregnated in a 40% phosphoric acid solution at a ratio of 1.5 g of acid per g of kernels. The impregnation was carried out in an oven at a temperature of 120 °C for 6 h. The impregnated grains were kept in hermetically sealed flasks until the carbonization (pyrolysis) tests [35] and then carbonized in a furnace (muffle furnace model: Nabertherm P330) and fired in a borosilicate glass crucible at a temperature of 450 °C with a heating rate of 7.5 °C/min and a 2 h isotherm step. The resulting activated carbon was cooled at room temperature in a desiccator. After acid activation, the product was washed with 0.1 mol·L⁻¹ of hydrochloric acid to remove the impurities. Then, the product was washed with distilled water until a pH value of 6.5 was achieved and dried in an oven at 105 °C for at least 8 h [32,36]. The different steps in the synthesis of activated carbon (BA-AC) are shown in Figure 1.

Characterization of activated carbon

Before arsenic (III) adsorption tests were conducted, the BA-AC was fully characterized through several physicochemical measurements. The Brunauer–Emmett–Teller (BET) analysis and Barret–Joyner–Halenda (BJH) isotherm (ASAP 2020 accelerated surface area and porosimetry system from Micromeritics Norcross GA, USA) made it possible to determine, respectively, the specific surface areas and the pore volumes and sizes of the activated carbon (BA-AC) samples. The morphological characterization of the BA-AC samples was achieved by scanning electron microscopy (SEM) (HITACHI SU8020, computer-controlled with the EDX SDD software, Thermo Scientific, Mons, Belgium). To characterize the adsorbent material, BA-AC, X-ray powder diffraction (XRPD) was carried out using a D8 Advance Davinci Bruker X-ray generator diffractometer (working at a 40 mA generator current and a 40 kV generator voltage with Cu-K α radiation ($\lambda = 1.54060$ Å)). The XRPD data were recorded at a scanning speed of 0.02° s⁻¹ and at 2 θ angles with values ranging from 5° to 70°.

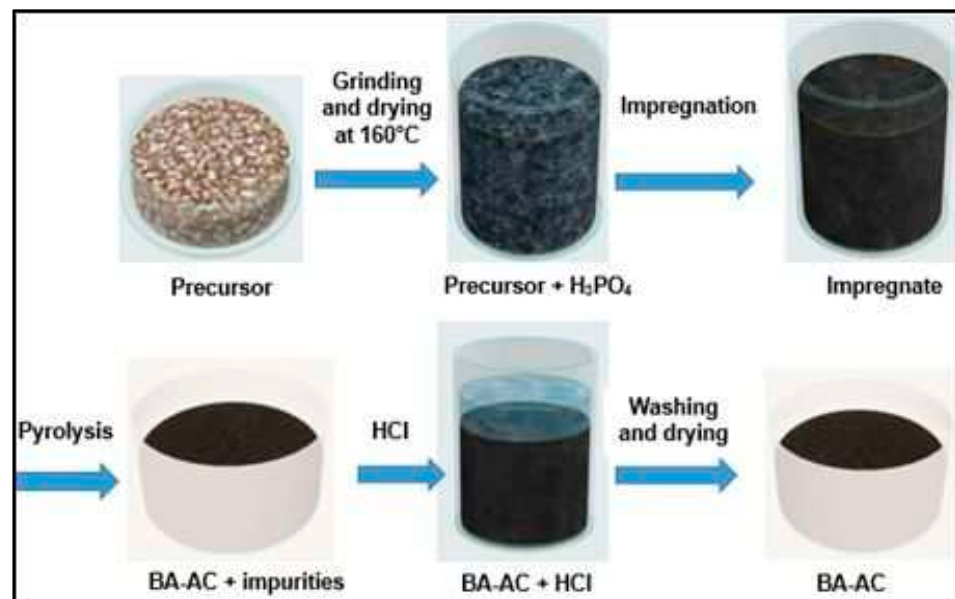


Figure 1. Steps in the synthesis of activated carbon (BA-AC).

2.3.2. Fixed-Bed Column Investigations

Column Experimental Set Up

The studies on the columns were carried out in two steps. In the first step, a glass column with a diameter of 7 cm was packed with only DA laterite or activated carbon (BA-AC). A second set of experiments was carried out with a column filled with DA laterite interspersed at 25% of the total height of the bed by either BA-AC (DA/BA-AC) or fine sand BD (DA/BD), distributed in five layers of equal height. The characteristics of the sand sample are given in the Supplementary Materials (SI3). For the column packed with only DA laterite, the tests were performed at different depths (20, 30, and 40 cm) and with different particle sizes ($0.900 \leq G_1 < 1.250$ mm and $0.425 \leq G_2 < 0.900$ mm). For the second column (DA laterite–BA-AC), the tests were conducted under different experimental conditions, such as bed depths of 20, 30, and 40 cm and initial concentrations of 0.5, 1, and 2 mg/L, to determine the effects.

The As(III) solutions were stored in 20 L canisters, which had hand taps suitable for rural areas, and introduced into the fixed-bed column in the down-flow mode through the column at a constant flow rate of 50 mL/min. This flow rate was chosen to provide a sufficient amount of effluent per minute that is acceptable on a field scale (Supplementary Information (SI4)).

To avoid migration and floating by the adsorbents and to allow for a uniform distribution of the solution through the column, glass wool was placed on both sides of the column. Treated As(III) samples were collected in 40 mL tubes at regular intervals and analyzed using an electrochemical method developed by Sakira et al. [6].

The determination of As(III) was carried out using a mini potentiostat (910 PSTAT mini Metrohm) driven by the 910 PSTAT software. The device included a 10 mL plastic cell held in place by a ring in which a carbon paste electrode modified by gold nanoparticles (Au-NP/CPE); a silver chloride reference electrode (Ag/AgCl); saturated KCl (208 mV potential at 25 °C compared to the normal ENH hydrogen electrode); and a platinum auxiliary electrode were placed. The carbon paste electrode modified by gold nanoparticles (Au-NP/CPE) was prepared by introducing a paste composed of 60% graphite and 40% solid paraffin followed by a physicochemical and electrochemical modification [6]. The As(III) concentrations were determined by Differential Pulse Anodic Stripping Voltammetry (DPASV) in a potential range of -0.3 to 0.3 V/ECS after a pre-concentration time of 180 s by introducing 10 mL of filtrate into the cell containing the three electrodes in a hydrochloric acid medium (HCl, 1 M). The detection limit was estimated to be 0.932 µg/L. Previous studies on the physicochemical characterization of drilling waters in the northern region of

Burkina Faso (in the village of Tanlili where the filtration device is currently implemented) revealed an average As(III) concentration of 1.99 ± 0.06 mg/L [21]. This concentration, which was determined in the field of measurements, constituted our reference point. Therefore, the maximum concentration of As(III) for the fixed-bed adsorption experiments was set at 2 mg/L during our laboratory experiments.

The column was considered to be exhausted when the effluent concentration was greater than 10 µg/L (WHO guide). All experiments were performed at room temperature. The experimental setup is presented in Figure 2.

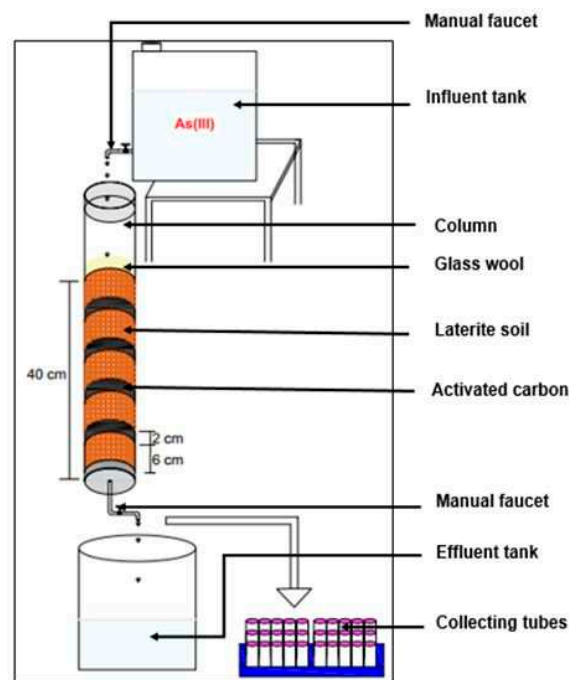


Figure 2. Experimental device for solution percolation through natural laterite fixed-bed column with alternating activated carbon layers (DA/BA-AC).

Fixed-Bed Column Data Analysis

The analysis of the column data was performed according to the literature [37]. The escape time (t_e) is defined as the point on the breakthrough curve at which adsorbate is detected at the outlet of the column, whereas the breakthrough time (t_p) is the point on the curve where the arsenic concentration reaches its maximum allowable value of 0.01 mg/L [38]. The column was considered to be at the breakthrough point when the arsenic (III) concentration at the column outlet reached the maximum allowable level (0.01 mg/L) [39].

A breakthrough curve is usually expressed as $\left(\frac{C_t}{C_0}\right)$ and as a function of time or volume treated for a given bed depth.

The processed volume (V) (mL) can be calculated using Equation (2) as follows:

$$V(\text{mL}) = Q \times t_{tot} \tag{2}$$

where Q and t_{tot} are the volumetric flow rate (mL/min) and the total flow time (min), respectively.

The total amount of arsenic adsorbed in the column (q_{tot} (mg)) is calculated from the area under the breakthrough curve using Equation (3) [38]:

$$q_{tot}(\text{mg}) = \frac{Q}{1000} \int_{t=0}^{t=tot} C_{ad} dt = \frac{Q}{1000} \int_{t=0}^{t=tot} (C_0 - C_t) dt \tag{3}$$

where C_{ad} is the concentration of arsenic adsorbed at time t , C_0 is the initial arsenic concentration, and C_t is the arsenic concentration at time t . All concentrations are in mg/L.

The maximum equilibrium arsenic adsorption capacity of the column ($q_{eq} \left(\frac{mg}{g} \right)$) is calculated using Equation (4) [40] as follows:

$$q_{eq} \left(\frac{mg}{g} \right) = \frac{q_{tot}}{m} \tag{4}$$

where m is the mass (in g) of the adsorbent in the column.

The total amount of arsenic introduced into the column is calculated using Equation (5) [38] as follows:

$$m_{tot} (mg) = \frac{C_0 \times Q \times t_{tot}}{1000} \tag{5}$$

The percentage of arsenic removed $R(\%)$ can be obtained using Equation (6) [38] as follows:

$$R(\%) = \frac{q_{tot}}{m_{tot}} \times 100 \tag{6}$$

Bohart–Adams model and Bed Depth Service Time (BDST) model

To facilitate the scale up of the process without being too expensive, to predict the results instead of having to conduct experiments in the laboratory, and to avoid important delays in the realization of the experiments, we modeled the columns using two theoretical models, namely, the Bohart–Adams model and the Bed Depth Service Time (BDST) model.

Bohart–Adams model

The Bohart–Adams model is described using Equation (7) [39]:

$$\ln \left(\frac{C_t}{C_0} \right) = K_{AB} \times C_0 \times t - K_{AB} \times N_0 \times \left(\frac{Z}{U_0} \right) \tag{7}$$

where C_0 (mg/L) is the initial arsenic concentration; C_t (mg/L) is the arsenic concentration at the column outlet at time t (mn); K_{AB} is the Bohart–Adams kinetic constant ($\frac{L}{mg \cdot mn}$); N_0 is the saturation concentration, or mass capacity (mg/L); Z is the height of the fixed-bed column (cm); and U_0 is the surface velocity (cm/mn), which is defined as the ratio of the volumetric flow rate (Q) (cm^3/mn) and the cross-sectional area (A) (cm^2) of the bed.

Bed Depth Service Time (BDST) model

The Bohart–Adams model has been used by various authors [38,39], and its developments and/or approximations lead to determinations of the adsorption capacity at saturation, values of the rate constants, and speed of movement of the adsorption front. The below equation is that of Bohart–Adams combined with that of Thomas [39], and it is represented by Equations (8) and (9) [39] as follows:

$$\ln \left(\frac{C_0}{C_t} - 1 \right) = K_B \times N_0 \times \left(\frac{Z}{U_0} \right) - K_B \times C_0 \times t \tag{8}$$

Hence,

$$t = \frac{N_0}{C_0 U_0} Z - \left(\frac{1}{C_0 K_B} \right) \ln \left(\frac{C_0}{C_t} - 1 \right) \tag{9}$$

where C_0 (mg/L) is the initial solute concentration, C_t (mg/L) is the desired solute concentration at a defined breakthrough time, K_B is the adsorption rate constant ($L/(mg \cdot h)$) in hours, N_0 is the adsorption capacity (mg/L), Z is the column depth (cm), and t is the length of the operating time of the column (h).

By fixing $t = 0$ and solving Equation (9), we obtain Equation (10) as follows:

$$Z_0 = \left(\frac{U_0}{N_0 K_B} \right) \ln \left(\frac{C_0}{C_t} - 1 \right) \tag{10}$$

In this technique, called the BDST (bed depth service time) approach, the Bohart–Adams equation is expressed by Equations (11)–(13) [39] as follows:

$$t = az + b \quad (11)$$

$$a = \frac{N_0}{C_0 U_0} \quad (12)$$

$$b = -\left(\frac{1}{C_0 K_B}\right) \ln\left(\frac{C_0}{C_t} - 1\right) \quad (13)$$

This equation allows us to determine the theoretical operating times of the column by studying the influence of the bed depth.

2.3.3. Hydraulic Conductivities

The characterization of both intercalated and non-intercalated laterite can be conducted by investigating the modification of a specific physical property. We chose hydraulic conductivity as its measurement can be carried out at a low cost and it is easy to implement. The hydraulic conductivities of the non-intercalated fixed-bed systems (i.e., laterite fixed-bed column and activated carbon (BA-AC) fixed-bed column) and the intercalated laterite fixed-bed columns were determined by Darcy's law using a constant head permeability meter with a 20 cm height (L) for the material layer and a 7 cm diameter. The water was allowed to flow downward through the material, and the flow rate (Q) was measured. The hydraulic conductivity or permeability coefficient, K (cm/s), was determined using Equation (14) [41]:

$$K = \frac{Q \times L}{A \times \Delta H} \quad (14)$$

where Q is the flow rate (cm³/s); K is the saturated hydraulic conductivity or permeability coefficient (cm/s); ΔH is the hydraulic head pressure (cm); L is the length of the material layer (cm); and A is the cross-sectional area of the column (cm²).

The infiltration rate of the water was determined using Equation (15) [41]:

$$v = \frac{Q}{A} = K \times i \quad (15)$$

where i represents the imposed hydraulic gradient without a unit, which is determined using Equation (16) [41]:

$$i = \frac{\Delta H}{L} \quad (16)$$

The measurements of the hydraulic conductivities of the non-intercalated laterite bed and intercalated laterite bed provided data that confirmed the intercalation in the fixed-bed system.

2.4. Statistical Analysis

The fitting of the data for the percolation adsorption and the standard deviation of the free swelling index of the DA laterite were carried out using Excel (Microsoft Excel 2016). Differences were considered significant at a p -value < 0.05.

3. Results and Discussion

3.1. Free Swelling Index of DA Laterite

Figure 3 shows that the free swelling index increased with the depth (Z) of the fixed-bed column. It also shows that the swelling index evolved with the duration of the wetting, and it stabilized after 24 h. In fact, it can be observed that the free swelling index increased from 23.26 to 28.03% when the bed height increased from 5 to 15 cm. This increase in the swelling index was certainly due to the presence of a significant amount of swelling

minerals or clayey parts. The swelling was mainly related to the mineralogical nature of the clays [40].

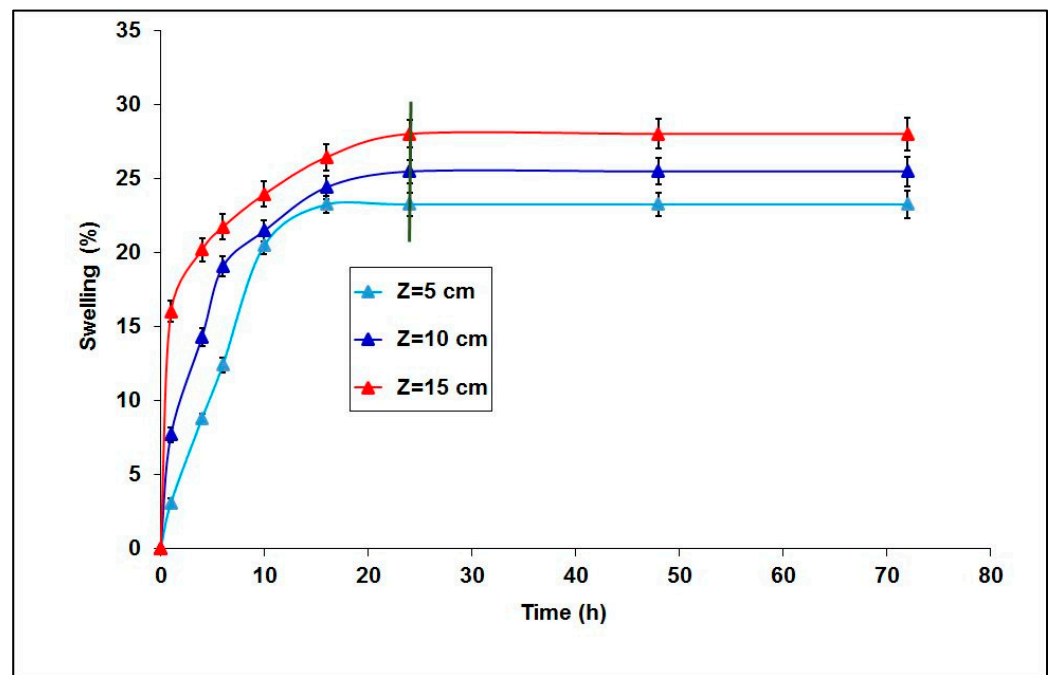


Figure 3. The free swelling index as a function of time.

3.2. Characterization of Activated Carbon

3.2.1. Physicochemical Characteristics

Knowledge of the physicochemical characteristics of carbon (thermal and/or chemically activated) is necessary to understand many phenomena, such as adsorption, desorption, ion exchange, and others [31,32]. Phosphoric acid is the best impregnation reactant used in most cases, including the activation of carbon. According to the literature, the result of impregnation is the formation of C–O–P bindings at active carbon surface sites, which lead to activated carbon with a high specific surface area [34].

The results of the characterization are summarized in Table 3. It can be noticed that BA-AC has a suitable specific surface area and porosity for the adsorption of As(III). The specific surface area value of BA-AC, as determined by the BET method, was 666.46 m²/g. This value is greater than most in the reported literature, which have values in the range of 155–598 m²/g [23,42] and a biochar value in the range of 188–543 m²/g [43]. The adsorption–desorption isotherms for nitrogen (N₂) at 77 K are shown in Figure 4. This value is significantly high compared to the values reported in the literature, which are in the range of 520–876 m²/g for activated carbon synthesized from local biomass in the context of As(III) adsorption [32,44,45]. It can also be noted that BA-AC had a relatively small average pore diameter (2.78 nm), almost reaching the limit for microporosity, and a large micropore volume (0.2720 cm³/g). Figure 5 shows the pore size distribution curves of the activated carbon (BA-AC).

The sizes of these pores, which are less than 2 nm, and the small total pore volume confirm activated carbon's microporous nature, as defined by the International Union of Pure and Applied Chemistry (IUPAC)'s classification of pore size ranges [34].

The iodine and methylene blue indices, which were used to determine the nature of the dominant pores of activated carbon, were 15.44 mg/g and 869.95 mg/g, respectively. The highest value of the iodine index resulted from a predominance of micropores, and it contributed to the increase in the adsorption capacity of BA-AC [34,36].

Table 3. Physicochemical characteristics of activated carbon.

Parameter	Value
C (%)	80.00
Iodine number (mg/g)	869.95
Methylene blue number (mg/g)	1.32
Surface area (S_{BET}) (m^2/g)	666.46
Micropore surface area (S_{mic}) (m^2/g)	610.70
Total pore volume (V_p) (cm^3/g)	0.27
Average pore diameter, by BET (nm)	2.78
Average pore diameter, by BJH (nm)	2.97

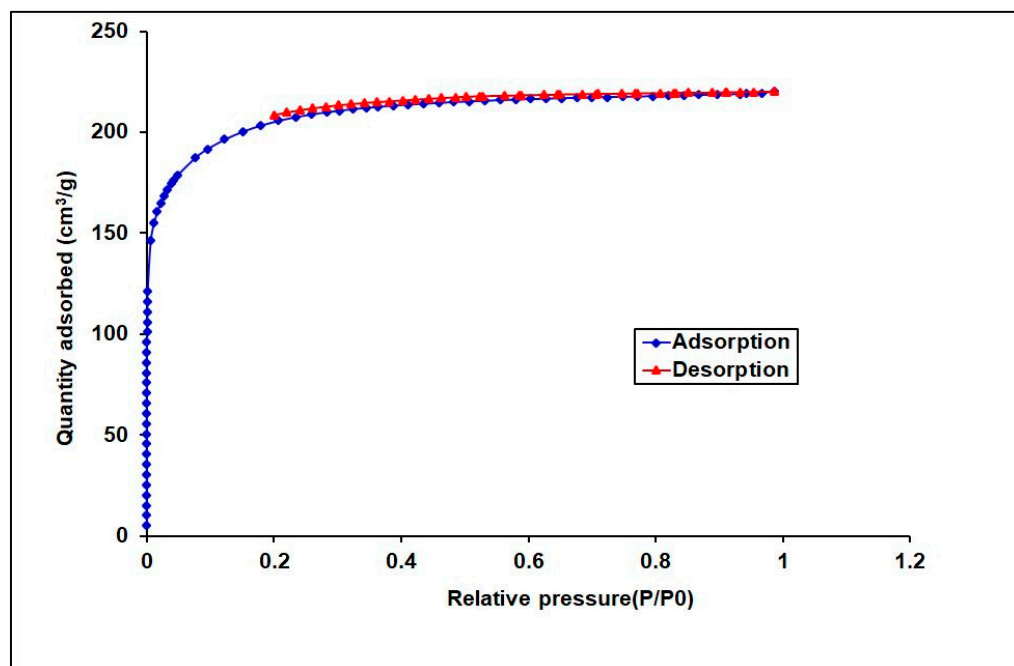


Figure 4. Adsorption–desorption isotherm curves of nitrogen (N_2) at 77 K for BA-AC.

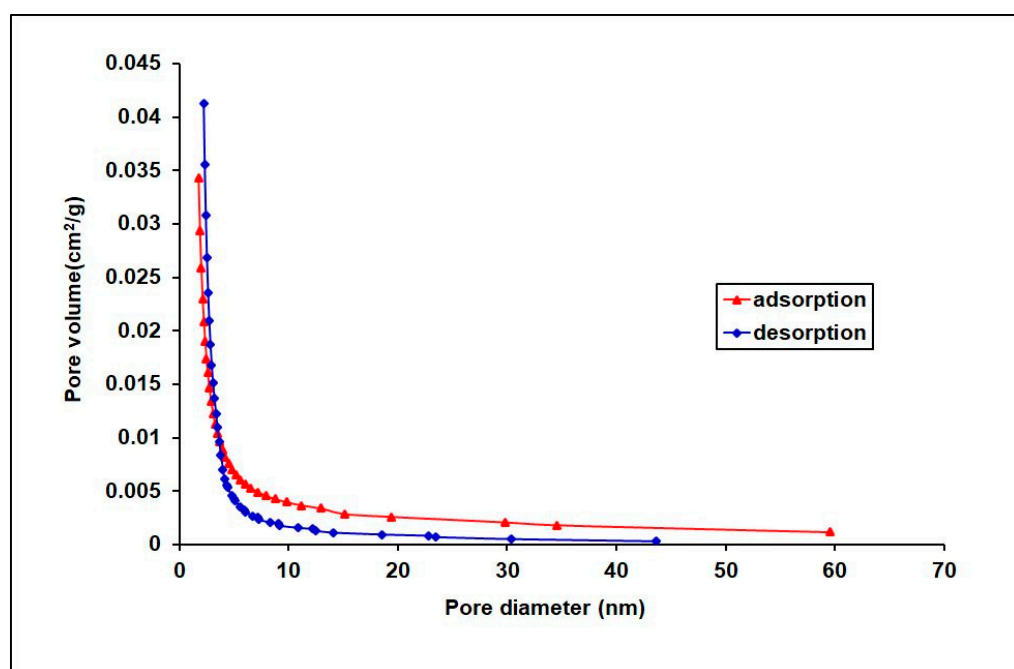


Figure 5. Pore size distribution curves of activated carbon (BA-AC).

3.2.2. Structural Characteristics

The diffractogram of the activated carbon (Figure 6) did not show a crystalline phase. This clearly indicates that BA-AC was characterized by an amorphous structure with no detectable crystallized species on its surface, as reported in the literature [31,45]. This amorphous structure has a huge advantage regarding pollutant adsorption. Indeed, well-prepared activated carbon mainly has an amorphous structure, which is highly porous, exhibiting a broad range of open pore sizes of molecular dimensions, and it is appropriate for pollutant adsorption by column percolation. The amorphous structure was confirmed by an SEM analysis.

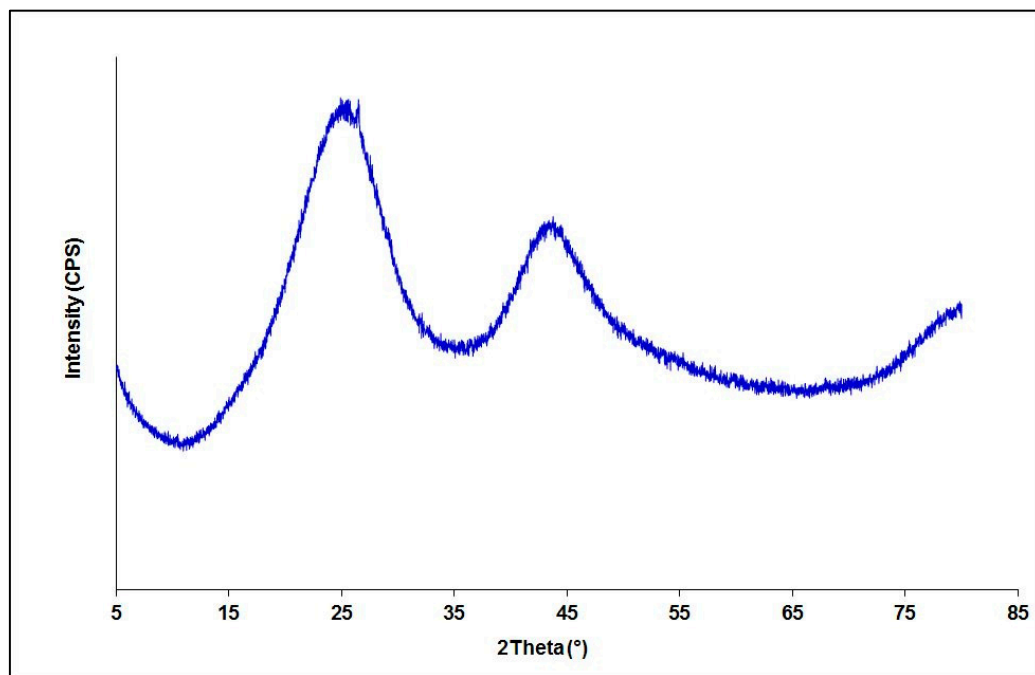


Figure 6. Diffractogram of BA-AC.

The SEM analysis shows the nature of the pores on the BA-AC particles' surfaces (Figure 7). The SEM images in Figure 7c,d were characterized by a similar porous morphology, whereas those in Figure 7a,b show relatively more homogeneous pores with constant diameters. Pore-like capillary cracks can be observed in Figure 7a–c. These cracks are of different sizes, and inside the larger ones, additional cracks with smaller diameters are observed. These results indicate that BA-AC was characterized by significant porosity and pores of different sizes [12].

The results of the EDX analysis allowed for the elemental analysis of BA-AC. It was observed that BA-AC contained mainly carbon and oxygen atoms in small quantities. This result confirms that BA-AC was a strongly carbonaceous material at 85%. Other atoms that were present, such as oxygen (11.75%), phosphorus (2.85%), and trace amounts of calcium, were either from the composition of the raw material or from the activating agent. The presence of phosphorus atoms may have resulted from the reaction of phosphate ions with the raw material [7].

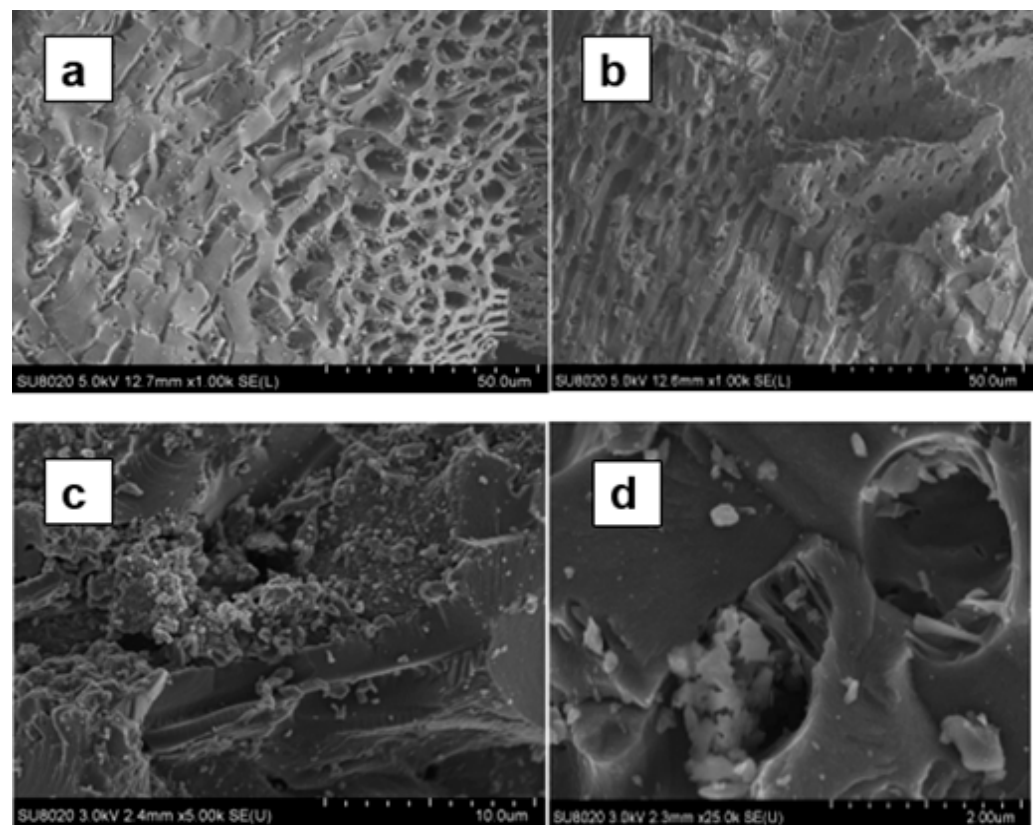


Figure 7. SEM images of BA-AC grains magnified at (a) 50 μm ; (b) 50 μm ; (c) 10 μm ; and (d) 2 μm .

3.3. Investigation of Fixed-Bed Column Packed with Only DA Laterite

3.3.1. Effect of Bed Height on Clogging

An appreciation in the column clogging by laterite particles as a function of the bed height was inferred from a decrease in the affluent flow rate as a function of time. Figure 8 shows that the bed height favored the compaction of the laterite, leading to the risk of clogging; the higher the bed height, the higher the risk. The interruption time was defined as the time elapsed from the start of percolation to clogging when the effluent stopped percolating through the column. These interruption times for 30 and 40 cm bed heights were equal to 7 and 3 h, respectively. However, with a bed height of 20 cm, the breakthrough occurred without the clogging of the adsorptive porous system by laterite particles during the percolation process. Indeed, we noticed that for the 30 and 40 cm bed heights, a large number of fine particles exhibited a high swelling rate compared to those for a 20 cm height (Figure 8). The observed clogging phenomena for these bed heights (30 and 40 cm) can be explained by the fact that a greater bed depth favors the development of a stilling zone. The latter served as a deposition site for fine particles, resulting in a decrease in the water load passing through the layers. As a matter of fact, in the case of the fixed-bed column filled with only laterite particles, the use of greater bed depths, aimed at achieving a better adsorption capacity and a longer breakthrough time, always resulted in column clogging in the long run, which is in contrast to the results reported in the literature when only small laboratory columns were used in the experiments [19,24]. To overcome this issue of clogging that occurs for greater bed depths, the method of using alternating layers (laterite layers alternated with layers of either an adsorbent material or an inert material) was examined in the subsequent investigations.

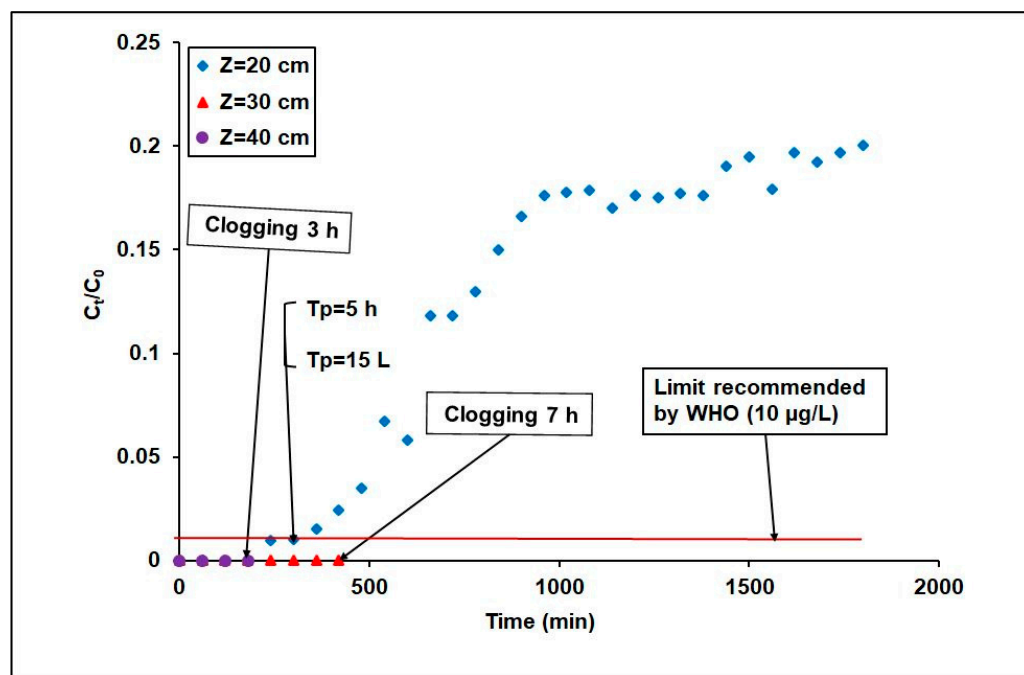


Figure 8. Breakthrough curves of As(III) adsorption in DA-laterite-packed column at different bed depths ($[As(III)]_I = 1 \text{ mg/L}$; flow rate = 50 mL/min; diameter = 7 cm; grain size = $0.900 \leq G \leq 1.250 \text{ mm}$).

3.3.2. Effect of Particle Size on Clogging

The study of column clogging by laterite particles as a function of the laterite particle size is illustrated in Figure 9. It can be seen that the reduction in the laterite particle size accentuated column clogging by the laterite particles. This can be explained by the fact that there were more fine particles in the column ($0.425 \leq G_2 < 0.900 \text{ mm}$), leading to a high swelling rate. Because the fine laterite particles contained a significant amount of oxide Fe_2O_3 (20.4%), it seems reasonable to foresee electromagnetic phenomena that could occur between the surface of the laterite grains and the iron particles. This may generate a deposition layer by adsorption on the grain surfaces [46]. These electromagnetic phenomena that occur between the surface of the laterite grains and the iron particles, combined with the deposition of fine particles on the surface of the porous structure, were likely the cause of the progressive clogging of the interstices of the laterite layers. For the efficient operation (i.e., without clogging) of the adsorptive porous system during the percolation process, the intercalation of layers with a non-swelling material (adsorbent or inert) was further considered.

The results presented in Sections 3.3.1 and 3.3.2 clearly show that two factors likely combine to accentuate clogging during water percolation in a fixed-bed column. The first is the nature of the percolator material, which may be subjected to a permeability issue due to the small size of the particles. Just like clay minerals, laterite soil is composed of small particles less than $2 \mu\text{m}$ in size, which place them within the limits of the colloidal state. This results in physicochemical properties that combine a high specific surface area and electric charges on the basic silicate structure, favoring the deposition of suspended fine particles on the outer surface or within the pores of the laterite’s porous structure (i.e., blockage of pores by fine particles). The second factor is the fact that a higher bed leads to the development of a deposition zone favoring cake formation by fine particles. It should be noted that this phenomenon is not limited to only lateritic soils. As part of our investigations, we assessed clogging with other types of natural swelling materials such as local bentonite and smectite (Supplementary Information (SI1)). Consequently, one of the best ways to avoid clogging by fine particles when working with bed heights greater than 20 cm is, precisely, to reduce the bed height, which is favorable to a deposition of fine particles, by intercalating the layers of swelling material with adsorbent or inert material

layers. This constitutes the fundamental basis of the alternating layer method, which is developed in the present work. However, another effect was sought with the alternating layer method. This involved the intercalated material increasing the permeability of the whole system compared to the initial laterite fixed-bed column. This condition must be met to achieve a better performance by the fixed-bed column.

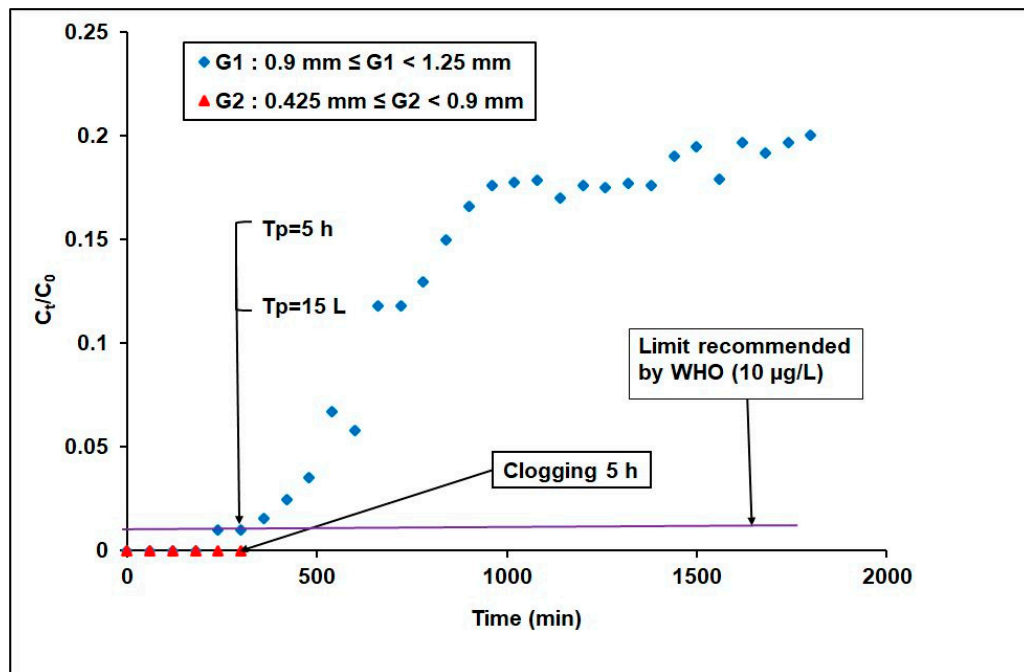


Figure 9. Breakthrough curves of As(III) adsorption in column packed with laterite with different particle sizes ($[As(III)]_i = 1 \text{ mg/L}$; flow rate = 50 mL/min; diameter = 7 cm; bed height = 20 cm).

3.4. Investigation of Column Packed with Alternating Layers of Laterite

3.4.1. Comparative Study of Three Fixed-Bed Columns: Packed with Only Laterite (DA), Laterite Intercalated with Activated Carbon (DA/BA-AC), and Packed with Only Activated Carbon (BA-AC)

Dynamic mode retention tests of arsenic (III) in the three columns with an identical bed height (20 cm) resulted in breakthrough times of approximately 5, 15, and 19 h for the columns packed with only laterite, laterite intercalated with activated carbon, and only activated carbon, respectively (Figure 10); in addition, their adsorption capacities were 0.0173 mg/g, 0.0530 mg/g, and 0.127 mg/g, respectively (Table 4). These results confirm that the column packed with only activated carbon and the one packed with laterite intercalated with activated carbon had better performances than the one packed with non-intercalated laterite. These results also confirm that the column filled with only activated carbon was more efficient than the one filled with laterite intercalated with activated carbon.

Table 4. Fixed-bed column parameters for adsorption of As(III) in columns packed with only laterite, laterite intercalated with activated carbon, and only activated carbon.

Materials	Mass (kg)	t_p (min)	V_p (L)	Q_{tot} (mg)	Q_p (mg/g)	R (%)
Non-intercalated laterite bed	0.858	300	15	14.85	0.0173	99
Laterite bed intercalated with activated carbon	0.839	900	45	44.55	0.053	99
Non-intercalated activated carbon fixed bed	0.444	1140	57	56.43	0.127	99

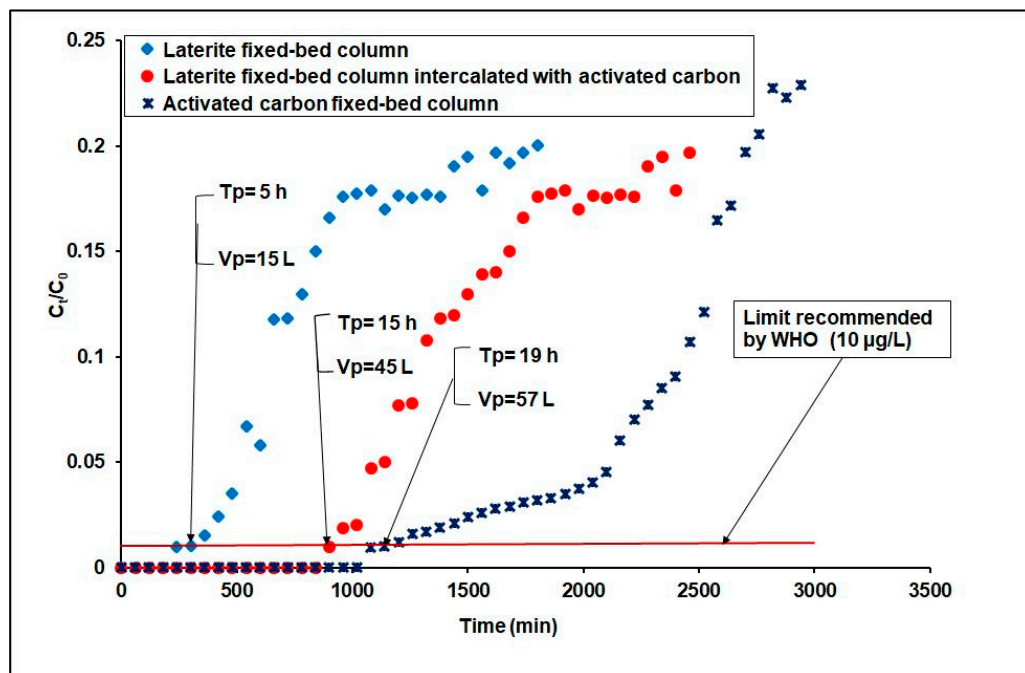


Figure 10. A comparison of the performances of the following three fixed-bed columns: non-intercalated laterite column, laterite fixed-bed column intercalated with activated carbon, and activated carbon fixed-bed column ($[As(III)] = 1 \text{ mg/L}$; flow rate = 50 mL/min; diameter = 7 cm; grain size = $0.900 \leq G \leq 1.250 \text{ mm}$; bed height = 20 cm).

3.4.2. Comparative Study of Three Fixed-Columns: Laterite Column Intercalated with Activated Carbon (DA/BA-AC), Laterite Column Intercalated with Fine Sand (DA/BD), and Laterite Column Intercalated with Gravel

Dynamic mode retention tests of arsenic (III) in two columns with an identical bed height (20 cm) resulted in breakthrough times of approximately 4 and 15 h for the column packed with laterite intercalated with sand and the one packed with laterite intercalated with activated carbon, respectively (Figure 11); in addition, their adsorption capacities were 0.0130 mg/g and 0.0530 mg/g, respectively (Table 5). These results confirm that the column packed with laterite intercalated with activated carbon had a better performance than the one packed with laterite intercalated with sand. However, for the laterite fixed-bed column intercalated with gravel layers, no satisfactory results were achieved. Indeed, this column configuration containing repeated layers of laterite and low-cost gravels resulted in clogging during water percolation (Figure S3, Supplementary Information (SI5)). As a result, this column configuration was not considered in further investigations.

Table 5. Fixed-bed column parameters for adsorption of As(III) in column packed with laterite intercalated with sand and column packed with laterite intercalated with activated carbon.

Materials	Mass (kg)	t_p (min)	V_p (L)	Q_{tot} (mg)	Q_p (mg/g)	R (%)
Laterite bed intercalated with activated carbon	0.839	900	45	44.55	0.053	99
Laterite bed intercalated with sand	0.913	240	12	11.88	0.013	99

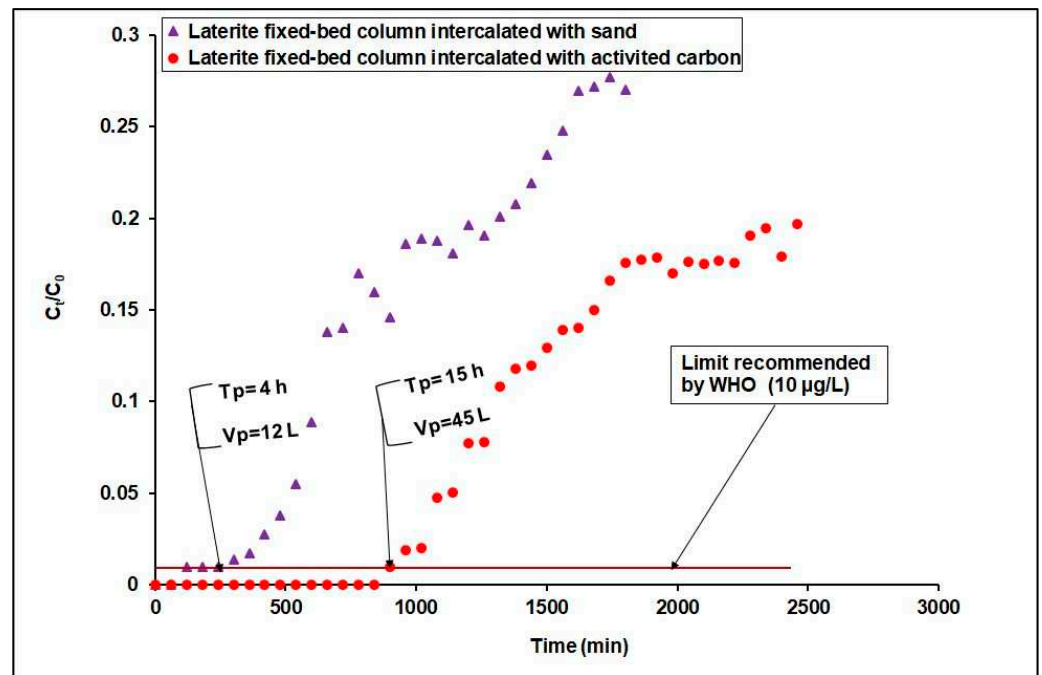


Figure 11. Comparison of performances of column packed with laterite intercalated with activated carbon and column packed with laterite intercalated with sand ([As(III)] = 1 mg/L; flow rate = 50 mL/min; diameter = 7 cm; grain size = $0.900 \leq G \leq 1.250$ mm; bed height = 20 cm).

3.4.3. Hydraulic Measurements

At this step, it is worth carrying out hydraulic measurements to determine why the laterite fixed-bed column intercalated with either activated carbon (BA-AC) or fine sand (BD sand) exhibited a better performance than the one with non-intercalated laterite (DA). The increase in the permeability to water of the porous system when we switched from the non-intercalated laterite to the intercalated laterite provides evidence of such a behavior. A Darcy law experiment was implemented to determine the hydraulic conductivity, or permeability constant (K), which represents the adsorptive porous system’s ability to transmit water [41]. The results obtained are shown in Table 6.

Table 6. Physical properties of adsorptive porous system.

Materials	A (cm ²)	Hydraulic Gradient, i	Q (cm ³ /s)	Hydraulic Conductivity or Permeability Coefficient, K (cm/s)
Non-intercalated laterite bed	38.4650	4.2500	0.3477	0.0021
Laterite bed intercalated with activated carbon	38.4650	4.2500	0.725	0.0044
Non-intercalated activated carbon fixed bed	38.4650	4.2500	35.285	0.215
Non-intercalated fixed-bed sand	38.4650	4.2500	18.466	0.1129
Laterite bed intercalated with sand	38.4650	4.2500	0.450	0.0027

Table 6 presents the permeability constants obtained for the following fixed-bed column configurations: non-intercalated laterite bed, laterite bed intercalated with activated carbon, non-intercalated activated carbon bed, laterite bed intercalated with sand, and non-intercalated sand bed. The permeabilities were 0.0021 cm/s, 0.0044 cm/s, 0.215 cm/s, 0.0027 cm/s, and 0.1129 cm/s, respectively. In silts, clayey sands, and laterite soils, the hydraulic conductivity is low, varying between 10^{-7} and 10^{-3} cm/s, whereas in clays, it varies between 10^{-11} and 10^{-7} cm/s, which makes them practically impermeable [47].

It can be noted that the intercalated laterite bed system presented a significant increase in permeability due to a higher flow velocity in comparison to the non-intercalated bed

system, which affected the permeability of the column. The main differences observed in terms of the permeability values could easily be related to the performances of the two column models, i.e., laterite fixed-bed columns intercalated with either activated carbon or fine sand.

Laterite is well known as a swelling material. On the basis of the literature, it is also known that intercalation of a swelling adsorbent with a non-swelling adsorbent material with a better hydraulic conductivity could improve the adsorptive porous system's permeability to water. As expected, the intercalated laterite bed exhibited a higher hydraulic conductivity compared to the non-intercalated laterite bed and, consequently, performed well. A higher hydraulic conductivity is linked to a higher flow rate and a lower residence time of the water inside the porous material, diminishing the risk of clogging. The hydraulic conductivity data not only allow us to assess the intercalation formation in the fixed-bed system, but also provide assurance that the intercalated laterite bed method can be applied in the removal of As(III). Consequently, the activated carbon and sand can be combined with the natural laterite in the water treatment process without any risk of clogging. So far, no permeability data have been reported for a natural laterite fixed-bed column intercalated with activated carbon. The present investigation provides data for an appropriate justification for the modification of the porous system's permeability when the laterite bed system is intercalated with either activated carbon or fine sand layers.

To summarize, the following fixed-bed column configurations can be used in treatments for arsenic (III) removal: packed with only activated carbon (BA-AC); packed with repeating layers of laterite and either activated carbon (DA/BA-AC) or fine sand (DA/BD). The performances are ranked in the following order: BA-AC > DA/BA-AC > DA/BD. We also made a comparison, in terms of the maximum adsorption capacity, between the following four systems: BA-AC, DA/BA-AC, DA/BD, and DA. It is noted from Tables 4 and 5 that the values are organized in the following order: BA-AC > DA/BA-AC > DA > DA/DB. As expected, the BA-AC system has an adsorption capacity value (0.127 mg/g) that is greater than that of the DA/BA-AC system (0.0530 mg/g). Although the laterite bed intercalated with sand (DA/DB) presents higher hydraulic conductivity than the non-intercalated laterite (DA), it is characterized by the lowest adsorption capacity value (0.0130 mg/g). Consequently, this system may not be suitable, compared to the BA-AC and DA/BA-AC systems, for the optimal adsorption of As(III). In the continuation of our analysis, we conducted a cost analysis of the BA-AC and DA/BA-AC column configurations, and the obtained results are presented in Table S2 (Supplementary Information (SI6)). Although the BA-AC column performed well, its cost (approximately USD 223.87) was far higher than that for the DA/BA-AC column (around USD 48.92). In the context of a rural environment and poverty, the column system with DA/BA-AC (repeating layers of alternating laterite and activated carbon (BA-AC)) is more appropriate than the BA-AC column system. In the present work, the subsequent investigations focus on the second column system (DA/BA-AC), which is more appropriate in terms of cost.

3.4.4. The Effect of the Bed Height on the Breakthrough Curve

Arsenic treatment with a DA-laterite-packed column alternated with BA-AC was studied as a function of the bed height (20, 30, and 40 cm) in a 7 cm diameter column. A synthetic As(III) solution of C_0 equal to 1 mg/L was used with a flow rate set to Q at 50 mL/min. In this study of arsenic (III) removal in the dynamic mode, the breakthrough curves ($C_t/C_0 = f(t)$) were plotted to determine the breakthrough time (Figure 12). Breakthrough was achieved when the arsenic concentration in the treated water was greater than or equal to the value of the limit (10 µg/L). The results are reported in Table 7.

It is noted that, contrary to the results presented in Figure 8, whereby an interruption of the percolation occurring for Z equals 30 and 40 cm, the combination of natural laterite and activated carbon allowed for the avoidance of clogging. Moreover, it can be seen (Figure 12) that with the increase in the bed height from 20 to 40 cm, the breakthrough time rose from 15 to 85 h, resulting in an increase in the volume of the treated As(III) solution

from 45 to 255 L. Indeed, a higher bed height contains a higher mass of the adsorbent, which requires a longer time to reach the saturation point and, thus, breakthrough [48]. This is in line with the data in Table 7, which indicate that the total amount of As(III) adsorbed increased from 44.450 to 252.450 mg when the bed height increased from 20 to 40 cm, respectively. These results highlight the fact that at a higher bed height, the mass or adsorbent surface increases, and consequently, the number of sorption sites that are likely to bind arsenic (III) increases [24,49]. As a result, we observed a greater adsorption capacity for As(III) as the bed height increased [21].

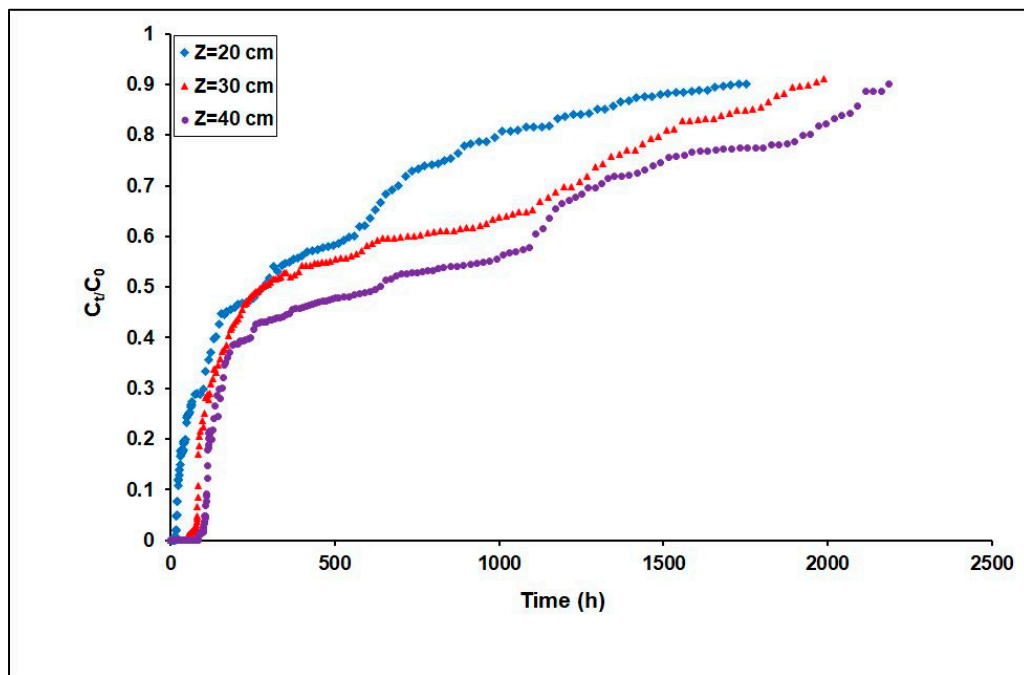


Figure 12. Breakthrough curves of As(III) adsorption in laterite-packed column intercalated with activated carbon at different bed depths ($[As(III)]_i = 1 \text{ mg/L}$; flow rate = 50 mL/min; diameter = 7 cm; grain size = $0.900 \leq G \leq 1.250 \text{ mm}$).

Table 7. Fixed-bed column parameters for adsorption of As(III) in DA-laterite-packed column intercalated with activated carbon at different bed depths.

Z (cm)	Mass (kg)	t_p (min)	V_p (L)	Q_{tot} (mg)	Q_p (mg/g)	R (%)
20	0.839	900	45	44.550	0.053	99
30	1.425	3360	168	166.320	0.116	99
40	1.780	5100	255	252.450	0.141	99

3.4.5. Dynamic Models

Modeling from Bohart–Adams Equations

The Bohart–Adams model was used to investigate the kinetics of arsenic removal in a column filled with DA laterite layers intercalated with BA-AC. The volumetric capacity (N_0) and the rate constant (K_{AB}) of the fixed-bed column system were determined, and their values are reported in Table 8.

Table 8. Bohart–Adams model parameters for As(III) adsorption in fixed-bed column system.

Z (cm)	Mass (kg)	N_0 (mg/L)	K_{AB} ($L \cdot mg^{-1} \cdot mn^{-1}$)	R^2
20	0.8390	12.3371	0.0023	0.8874
30	1.4250	6.2693	0.0015	0.9761
40	1.7800	2.7993	0.0014	0.9809

The coefficient of determination (R^2) (Table 8) increased from 0.887 to 0.980 when the bed height (Z) increased from 20 to 40 cm. The high value of the coefficient of determination ($R^2 = 0.980$ for a 40 cm bed height) indicates that, at this height, the Bohart–Adams model describes the experimental data satisfactorily. The increase in the bed height led to a decrease in both the K_{AB} and N_0 values, as already shown in previous investigations of As(III) adsorption [40,49]. In fact, increasing the bed height resulted in an increase in the contact time of arsenic (III) species with the DA laterite layers intercalated with activated carbon, which ultimately resulted in a better efficiency of the percolation process [48]. Thus, the decrease in the rate constant from 0.0023 to 0.0015 $L \cdot mg^{-1} \cdot min^{-1}$ when the bed depth increased from 20 to 40 cm suggested that the adsorption kinetics slowed down as a result of the increase in the adsorbent mass [50].

Application of BDST (Bed Depth Service Time) Mode

The experimental results obtained from the adsorption of As(III) by percolation in a column packed with DA laterite layers intercalated with BA-AC were fitted to the BDST model to determine the adsorption capacities and kinetic constants. It was previously reported that the breakthrough and saturation times corresponding to $C_t/C_0 = 0.01$, $C_t/C_0 = 0.2$, and $C_t/C_0 = 0.8$ were found to be 15 h, 55 h, and 85 h; 44 h, 87 h, and 120 h; and 1010 h, 1509 h, and 2080 h for bed depths of 20, 30, and 40 cm, respectively. In our context, the saturation point of the column was considered to be reached at $C_t/C_0 = 0.8$ (Supplementary Information (SI7)). Figure 13 shows the service time versus depth plot for 1, 20, and 80% saturations.

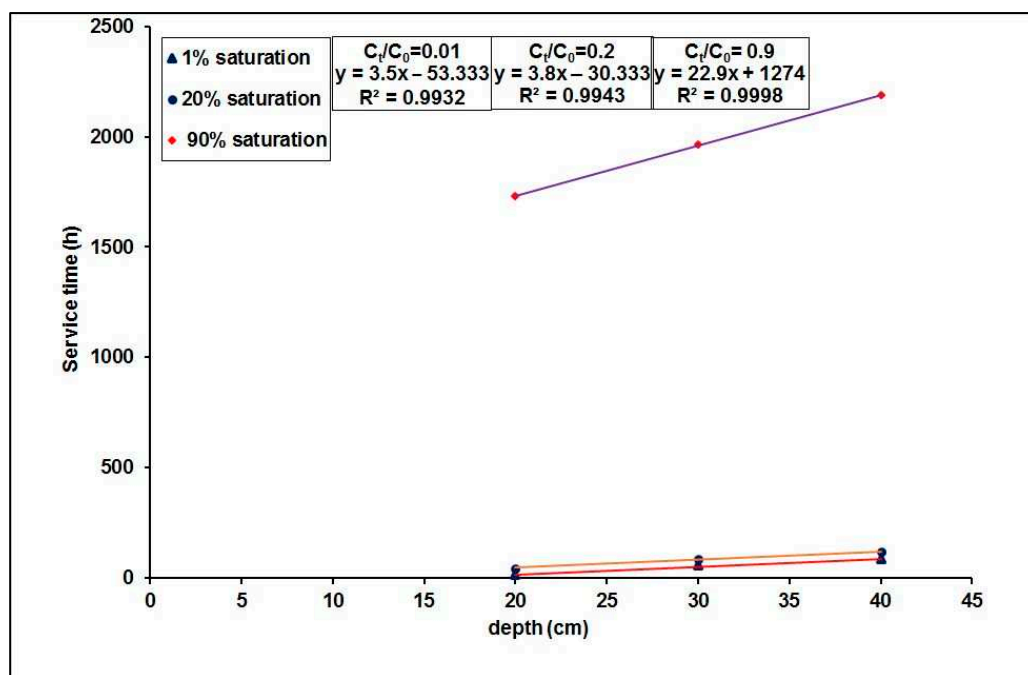


Figure 13. The evolution of service times (BDSTs) as a function of the different bed heights ($C_t = 1\% C_0$, $20\% C_0$, and $80\% C_0$).

From the slope and intercept of the 1, 20, and 80% saturation times, as shown in Figure 13, the design parameters N_0 and K_B were determined using Equations (12) and (13).

In Figure 13, it can also be seen that when the bed depth (Z) increased, the breakthrough time (t_p) also increased. This is related to the amount of adsorbent, which increased the adsorption capacity of the column. Finally, Figure 13 shows that the variation in the breakthrough times with the bed depth was linear, which validates the BDST model. The BDST parameters, such as the sorption rate constant (k_t), sorption capacity (N_0), and critical bed depth (Z_0), were calculated, and the results are summarized in Table 9.

Table 9. Bed depth service time (BDST) model parameters.

C_t	Z_0 (cm)	N_0 (mg/L)	K_B (L/mg·h)	R^2
1% C_0	15.230	1335.600	0.086	0.993
20% C_0	7.980	1450.080	0.046	0.994
80% C_0	1.340	20,415.600	−0.019	0.998

For 1, 20, and 80% saturations, it was observed (Table 9) that the determination coefficient values were all high ($R^2 = 0.99$). This proves that the results are consistent with the BDST model. There was also a steady increase in the slope from 3.5 to 53.5 when the breakthrough increased from 1 to 80% and a consistent increase in the coherent dynamic adsorption capacity (N_0) from 1335.60 to 20,415.6 mg/L of As(III). It is evident that after saturation at 1%, some active adsorbent sites were still available for As(III) adsorption. Similar observations were also reported by Podder et al. for a fixed-bed column filled with bacterial cells immobilized on a sawdust/MnFe₂O₄ composite [48]. It was shown that the slope increased from 0.0900 to 0.4300 and from 0.105 to 0.415 for As(III) and As(V), respectively, when the breakthrough increased from 1 to 20%. It was also observed by the authors that the coherent dynamic adsorption capacity (N_0) increased from 45.216 to 216.032 mg/L and from 52.752 to 208.496 mg/L for As(III) and As(V) removal, respectively [48]. Goel et al. also reported a slope increase from 12.50 to 35 for breakthrough values of 20–60% for the removal of lead using granular activated carbon [51].

The Bohart–Adams equation (i.e., BDST theory) assumes a rectangular isotherm with a constant dynamic adsorption capacity. All of these investigations recommend that the validation of the BDST model cannot be performed by only examining the coefficient of determination (R^2). The BDST model’s coefficients of a smaller breakthrough can still be used to estimate other parameters, such as the critical bed depth [48]. The critical bed depths estimated in our study were equal to 15.23 cm, 7.98 cm, and 1.34 cm for 1, 20%, and 80% breakthroughs, respectively. The rate constants calculated from the BDST graph intercept characterize the transfer rate of the solute from the liquid phase to the solid phase [52]. For this system, the high values found for the determination coefficient and the N_0 adsorption potential justify the high efficiency of the laterite fixed-bed column intercalated with activated carbon.

3.4.6. The Effect of the Initial Concentration of As(III) on the Breakthrough Curve

Because the arsenic contents present in borehole waters in the country are not constant, it is therefore necessary to investigate the influence of the initial As(III) concentration on the percolation process [53]. In order to establish the optimal performance of the continuous fixed-bed system, the effect of the initial As(III) concentration was studied by varying the concentration from 0.5 to 2 mg/L at a fixed flow rate of 50 mL/min and a bed height of 40 cm. Figure 14 shows that the adsorbent’s adsorption efficiency decreased with the gradual increase in the arsenic concentration in the influent. For example, the breakthrough times were 41, 85, and 204 h for 2, 1, and 0.5 mg/L of As(III) concentration, respectively. Similarly, the volume of treated water decreased from 612 to 123 L as the inlet As(III) concentration increased from 0.5 to 2 mg/L. A possible explanation for these results is that higher concentrations in the influent may lead to a more rapid mass transfer and the increase in the water’s ionic strength, allowing for the rapid diffusion of arsenite onto the adsorbent surface [54]. Consequently, a high concentration of arsenic in the tributaries leads to a reduction in the saturation time of the adsorbent [54]. In Table 10, it can be seen that when the initial concentration of As(III) at the inlet increased from 0.5 to 2 mg/L, the total amount of adsorbed As(III) (Q_{tot}) decreased from 299.268 to 245.870 mg, and the mass retention capacity (Q_p) decreased from 0.168 to 0.138 mg/g. A high concentration of As(III) provides a great driving force to overcome the fixed-bed column mass transfer resistance [55]. In this context, it is suggested that the adsorption sites were almost covered when the concentration of As(III) increased [55]. These results show that a change in

the concentration gradient substantially affects the saturation rate and the breakthrough time [44].

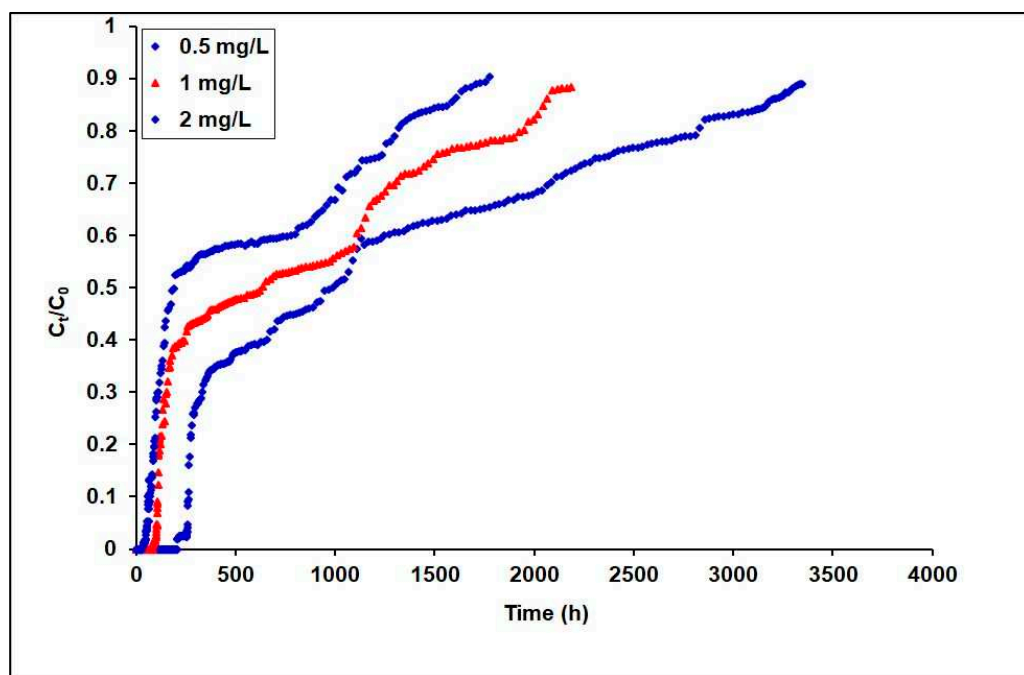


Figure 14. Breakthrough curves of As(III) adsorption in the laterite-packed column intercalated with activated carbon at different concentrations (bed depth (Z) = 40 cm; flow rate = 50 mL/min; diameter = 7 cm; grain size = $0.900 \leq G \leq 1.250$ mm).

Table 10. Fixed-bed column parameters for As(III) adsorption in DA-laterite-packed column intercalated with activated carbon at different concentrations.

C_0 (mg/L)	Q (mL/min)	Z (cm)	Mass (kg)	t_p (h)	V_p (L)	Q_{tot} (mg)	Q_p (mg/g)	R (%)
0.5	50	40	1.780	204	612	299.268	0.168	99
1	50	40	1.780	85	255	252.450	0.141	99
2	50	40	1.780	41	123	245.870	0.138	99

3.4.7. Changes in the Functional Groups of DA Laterite at the Breakthrough Point after the Adsorption of As(III)

The main functional groups on the surface of the raw DA laterite and As(III)-loaded DA laterite in the first (As(III) solution inlet layer) and fifth (bottom As(III) solution output layer) layers after column breakthrough were determined by FTIR (Figure 15). Figure 15 shows that the surfaces of all of the As(III)-charged laterites at the point of column breakthrough had similar major functional groups, such as Si-O-Fe (approximately 1100 cm^{-1}), Si-O-Si (1030 cm^{-1}), Al-OH (913 cm^{-1}), Fe-OH (798 cm^{-1}), and OH (in the 3730 cm^{-1} and 3100 cm^{-1} regions), as those of the crude DA laterite. In addition, the results show that the intensities of the FTIR spectra of the laterites in the two As(III)-loaded layers at the breakthrough point did not change compared with those of the raw laterite. This is due to the short interaction time between As and DA, which did not lead to the adsorption of larger quantities of As. The FTIR data on the DA residues at the breakthrough point are insufficient to assert that As(III) was chemically adsorbed onto the Fe- and Al-bearing minerals in the DA to elucidate the mechanism of As(III) adsorption by DA in the column. Similar results were already obtained by Nguyen et al. [24]. It is expected, however, that a change in the spectrum of the residues could be evident after the column is operated for a long period [24].

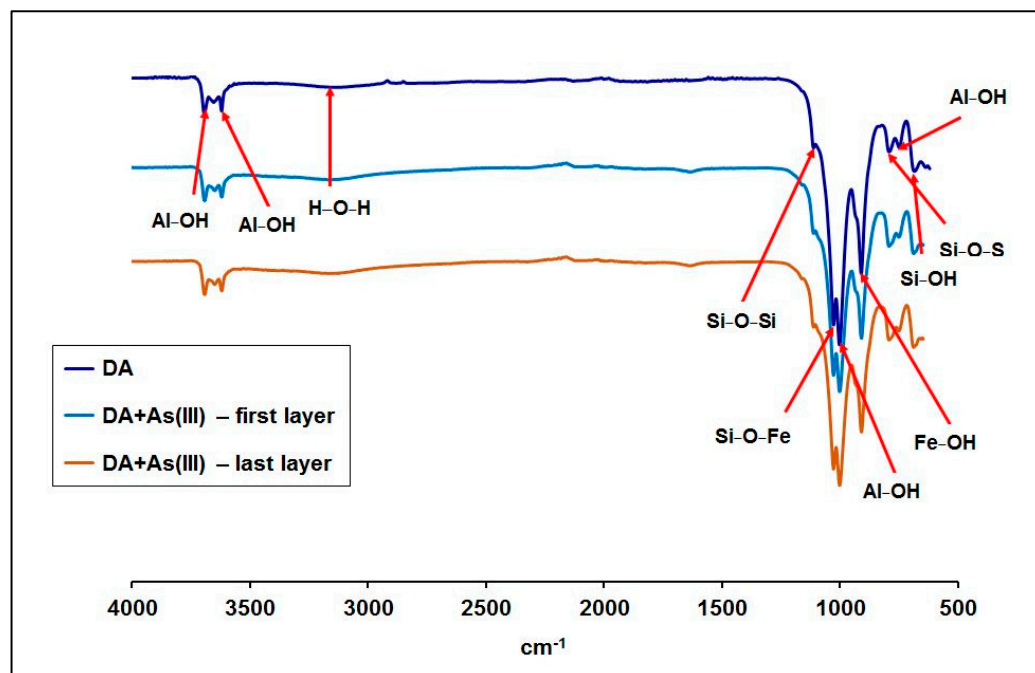


Figure 15. The FTIR spectra of the DA laterite before and at the point of breakthrough for As(III) adsorption.

3.4.8. A Comparison of the Adsorption Capacities Achieved for the Column Packed with DA Laterite Intercalated with Activated Carbon (Current Study) with Those Reported in the Literature

This study investigated the removal of As(III) in a fixed-bed adsorption process using a column packed with DA laterite layers intercalated with BA-AC layers. The obtained results clearly show that the column packed with laterite layers intercalated with BA-AC layers allowed for the avoidance of column clogging by laterite particles. Moreover, the process has the advantage of being applied for arsenic removal in real waters because of its ability to adapt to multiple processes, which can reduce treatment and operating costs. A comparison between this study and other studies reported in the literature on fixed-bed columns for arsenic adsorption is summarized in Table 11. From this table, it can be noted that the issue of column clogging by laterite particles in a fixed-bed column is envisaged for the first time in our study. It is also noted that the application of the alternating layer technique is promising, with a relatively long breakthrough time compared to other reported works [19,24,56]. A comparison of the Bohart–Adams adsorption capacity achieved in this study with those reported for other laterite adsorbents indicates that alternating DA laterite between BA-AC layers provided a higher adsorption capacity. According to the Adam’s modeling, to reach a maximum bed adsorption capacity (N_0) of 1335.6 mg/L of As(III) at a 1% breakthrough, a minimum critical bed depth of 15.23 cm is required. The modeling data are experimentally meaningful for a pilot treatment unit design. The optimal conditions for the efficient removal of As(III) are as follows: a minimum depth of the Z_{min} value set at 15.23 cm with an intercalated activated carbon height of 25%; a granulometry of the laterite ranging from 0.4 and 0.9 mm; and an adsorbent dose of As(III) ranging from 0.5 to 2 mg/L. It is anticipated that the data obtained on the laboratory scale may provide useful data that can be accurately applied in domestic and industrial systems.

Table 11. A comparison of the adsorption capacities achieved in the present study (a column packed with DA laterite intercalated with activated carbon) with those reported in the literature.

Adsorbent	Clogging	Adsorbat	Initial Concentration (mg/L)	Minimum Depth, Z_{min} (cm)	Adsorption Capacity (mg/L) *	T_P (h)	References
Laterite soil	-	As	0.33	-	-	6.75	[57]
Natural laterite (NL)	-	As(V)	1.00	9.11	67.00	24.00	[58]
Laterite soil	-	As(III)	0.50	-	108.02	32.00	[19]
Natural rocks coated with iron oxide (IOCNR)	-	As(III)	0.60	9.20	426.55	63.00	[59]
Natural laterite (NLTT)	-	As(V)	0.50	-	-	-	[24]
DA laterite	Clogging reported	As(III)	1.00	-	-	-	Present study
DA laterite + BA-AC	-	As(III)	1.00	15.23	1335.60	85.00	Present study

* Adsorption capacity corresponding to minimum depth (Z_{min}).

3.4.9. A Proposal of the Design of Household Arsenic Filters

On the basis of the results of the column test, we propose an alternative domestic filter based on DA laterite alternated with BA-AC activated carbon (Figure S4, Supplementary Information (SI8)) for the effective removal of arsenic and pathogens. The proposed filtration system would consist of a 1 m high column (including the thickness of the base) with an internal diameter of 15 cm. For the construction of the bed (bed height = 96 cm), the column would be filled with five layers of DA laterite of the same height (height of one laterite layer = 9 cm) interspersed at 25% of the total height of the bed, with BA-AC also distributed in five layers of the same height (height of one layer of activated carbon = 3 cm). To ensure that the filter operates correctly, maintenance must be carried out correctly, i.e., periodic cleaning of the filter on a monitored basis to ensure that the surface is available for arsenic adsorption and pathogen removal. The availability of mass-activated carbon for the local population can be achieved by a local project with a deposit of funds from national bodies. The transport and storage of laterite can be managed by the population in a warehouse. The replacement period for filter materials should be defined on the basis of pilot field trials to check the adsorption capacity and breakthrough time. These pilot tests are imperative to adjust the proposed dimensions and to determine the actual efficiency and performance of the filter. Field trials of the proposed filtration system are currently underway.

4. Conclusions

The adsorptive removal of As(III) through a laterite fixed-bed column intercalated with activated carbon layers synthesized from *Balanites aegyptiaca* kernels was performed with good efficiency. Permeability measurements were carried out for the following fixed-bed column configurations: non-intercalated laterite bed (DA), laterite bed intercalated with activated carbon (DA/BA-AC), non-intercalated activated carbon bed (BA-AC), laterite bed intercalated with sand (DA/BD), and non-intercalated sand bed (BD). The permeability data show that the intercalated laterite beds had a higher hydraulic conductivity than the non-intercalated laterite bed, resulting in good performances. The parameters of the laterite and intercalated laterite fixed-bed column were studied to determine the optimum experimental conditions. Adsorption experiments on the laterite fixed-bed column allowed us to confirm that the bed depth and particle size induced the clogging of the column with laterite particles. In contrast, column clogging was not dependent on the inlet concentration and flow direction. Investigations on the intercalated laterite beds showed that the laterite bed intercalated with activated carbon (DA/BA-AC) and the laterite bed intercalated with fine sand (DA/BD) solved the clogging problem, whereas the laterite bed intercalated with gravel led to clogging during percolation. Thus, by studying the effects of the initial concentration and bed height on the breakthrough curves of the most efficient system (DA/BA-AC), we found that the breakthrough time decreased with a rise in the initial concentration and increased with the bed height. On the basis of the Bohart–Adams equation, the BDST model was used to predict the relationship between the operating time and bed

height, which is essential in the design of a column adsorption process. The Bohart–Adams model was found to be highly representative. The BDST model, which was used to evaluate the column design parameters, showed a good fit with the experimental data. In view of the data obtained experimentally from the DA/BA-AC column configuration and the cost analysis of the column configurations (BA-AC and DA/BA-AC) (Supplementary Information (SI5)), the DA/BA-AC filtration system (DA laterite bed interspersed with activated carbon (BA-AC)) is a promising approach for treating arsenic-contaminated water that can be adapted to the living conditions of the rural population. These results are a step toward the large-scale use of this type of laterite-filled column intercalated with activated carbon to provide cleaner water in rural areas.

Supplementary Materials: The supplementary information can be downloaded at: <https://www.mdpi.com/article/10.3390/separations11040129/s1>. Figure S1. Breakthrough curve of As(III) for a fixed bed filled with the laterite adsorbent at different depths ($C_0 = 1.5$ mg/L and $Q = 3$ mL/min); Figure S2. Size distribution of BD sand; Figure S3. Laterite fixed-bed column intercalated with gravels layers; Figure S4. Proposal for a household filter based on DA laterite alternated with BA-AC activated carbon; Table S1. Main particle size parameters and uniformity coefficient for BD sand; Table S2. Cost of fixed-bed column configurations.

Author Contributions: Conceptualization, R.D.O., C.B., A.K.S., B.S. and B.G.; Methodology, R.D.O., C.B., A.K.S., B.S. and B.G.; Investigation, R.D.O. and C.B.; Writing—Original Draft Preparation, R.D.O.; Writing—Review and Editing, R.D.O., C.B., A.K.S., B.S., B.G., A.-L.H., E.Z., T.I.S., D.M., P.H. and J.-M.K.; Supervision, B.G., A.-L.H., E.Z., T.I.S., D.M., P.H. and J.-M.K.; Funding Acquisition, B.G., A.-L.H., E.Z., T.I.S., D.M., P.H. and J.-M.K. All authors have read and agreed to the published version of the manuscript.

Funding: The authors thank the ARES-CCD (Belgium), the Synergy 2018 project (Belgium), and the International Science Program (ISP, Uppsala, Sweden) for providing financial support.

Data Availability Statement: All data generated or analyzed during this study are included in this published article.

Acknowledgments: The authors thank the ARES-CCD (Belgium), the Synergy 2018 project (Belgium), and the International Science Program (ISP, Uppsala, Sweden) for providing financial support. The authors thank François Ouédraogo for participating in the helpful discussion regarding the measurement of hydraulic conductivity.

Conflicts of Interest: The authors declare no conflicts of interest.

References

1. Nasir, M.; Muchlisin, Z.A.; Saiful, S.; Suhendrayatna, S.; Munira, M.; Iqhrammullah, M. Heavy metals in the water, sediment, and fish harvested from the krueng sabee river aceh Province. *Indonesia. J. Ecol. Eng.* **2021**, *22*, 224–231. [[CrossRef](#)]
2. Khairunnash, A.; Muhammad, I.; Rayyan, R.D.; Aulia, A.; Qisthi, M.A.; Agnia, P.; Intan, Q.; Kana, A.S.N.P. Heavy metal contamination in aquatic and terrestrial animals resulted from anthropogenic activities in Indonesia. *Asian J. Water Environ. Pollut.* **2022**, *19*, 1–8. [[CrossRef](#)]
3. Glodowska, M.; Stopelli, E.; Thi, D.V.; Pham, T.K.T.; Pham, H.V.; Michael, B.; Andreas, K.; Sara, K. Arsenic behavior in groundwater in Hanoi (Vietnam) influenced by a complex biogeochemical network of iron, methane, and sulfur cycling. *J. Hazard. Mater.* **2020**, *407*, 124398. [[CrossRef](#)]
4. Liu, F.; Yang, W.; Li, W.; Zhao, G.C. Simultaneous oxidation and sequestration of arsenic (III) from aqueous solution by copper aluminate with peroxydisulfate: A fast and efficient heterogeneous process. *ACS Omega* **2021**, *6*, 1477–1487. [[CrossRef](#)] [[PubMed](#)]
5. Thangavel, S.; Balarama, V.; Mullapudi, K.; Kora, A.J.; Kumar, S. Covellite (CuS) as a novel adsorbent for the direct removal of As(III) and As(V) simultaneously from groundwater. *Sep. Sci. Technol.* **2021**, *57*, 683–697. [[CrossRef](#)]
6. Sakira, A.K.; Somé, I.T.; Ziemons, E.; Dejaegher, B.; Mertens, D.; Hubert, P.; Kauffmann, J.M. Determination of arsenic (III) at a nanogold modified solid carbon paste electrode. *Electroanalysis* **2015**, *27*, 309–316. [[CrossRef](#)]
7. He, X.; Deng, F.; Shen, T.; Yang, L.; Chen, D.; Luo, J.; Luo, X.; Min, X.; Wang, F. Exceptional adsorption of arsenic by zirconium metal-organic frameworks: Engineering exploration and mechanism insight. *J. Colloid. Interface Sci.* **2019**, *539*, 223–234. [[CrossRef](#)] [[PubMed](#)]
8. Ceballos-Escalera, A.; Pous, N.; Chiluiza-Ramos, P.; Korth, B.; Harnisch, F.; Bañeras, L.; Balaguer, M.D.; Puig, S. Electrobioremediation of nitrate and arsenite polluted groundwater. *Water Res.* **2021**, *190*, 116748. [[CrossRef](#)] [[PubMed](#)]

9. Garbinski, D.; Rosen, B.P.; Chen, J. Pathways of arsenic uptake and efflux. *Environ. Int.* **2019**, *126*, 585–597. [CrossRef]
10. Yaqub, M.; Lee, S.H. Experimental and neural network modeling of micellar enhanced ultrafiltration for arsenic removal from aqueous solution. *Environ. Eng. Res.* **2020**, *26*, 190261. [CrossRef]
11. Dhanasekaran, P.; Sahu, O. Arsenate and fluoride removal from groundwater by sawdust impregnated ferric hydroxide and activated alumina (SFAA). *Groundw. Sustain.* **2021**, *12*, 100490. [CrossRef]
12. Karki, S.; Timalisina, H.; Budhathoki, S.; Budhathoki, S. Arsenic removal from groundwater using acid-activated laterite. *Groundw. Sustain. Dev.* **2021**, *18*, 100769. [CrossRef]
13. Gong, X.J.; Li, Y.S.; Dong, Y.Q.; Li, W.G. Arsenic adsorption by innovative iron/calcium in-situ-impregnated mesoporous activated carbons from low-temperature water and effects of the presence of humic acids. *Chemosphere* **2020**, *250*, 126275. [CrossRef] [PubMed]
14. Alka, S.; Shahir, S.; Ibrahim, N.; Ndejiko, M.J.; Vo, D.-V.N.; Manan, F.A. Arsenic removal technologies and future trends: A mini review. *J. Clean. Prod.* **2021**, *278*, 123805. [CrossRef]
15. Türkmen, D.; Türkmen, M.; Akgönüllü, S.; Denizli, A. Development of ion imprinted based magnetic nanoparticles for selective removal of arsenic(III) and arsenic(V) from Wastewater. *Sep. Sci. Technol.* **2021**, *57*, 990–999. [CrossRef]
16. Li, Y.; Zhu, Y.; Zhu, Z.; Zhang, X.; Wang, D.; Xie, L. Fixed-bed column adsorption of arsenic(V) by porous composite of magnetite/hematite/carbon with eucalyptus wood microstructure. *J. Environ. Eng. Landsc. Manag.* **2018**, *26*, 38–56. [CrossRef]
17. Rahmi, R.; Lelifajri, L.; Iqbal, M.; Fathurrahmi, F.; Jalaluddin, J.; Sembiring, R.; Farida, M.; Iqhrammullah, M. Preparation, characterization and adsorption Study of PEDGE-Cross-linked magnetic chitosan (PEDGE-MCh) microspheres for Cd²⁺ removal. *Arab. J. Sci. Eng.* **2022**, *1*, 159–167. [CrossRef]
18. Maiti, A.; DasGupta, S.; Basu, J.K.; De, S. Batch and column study: Adsorption of arsenate using untreated laterite as adsorbent. *Ind. Eng. Chem. Res.* **2008**, *47*, 1620–1629. [CrossRef]
19. Maji, K.S.; Pal, A.; Pal, T.; Adak, A. Modeling and fixed-bed column adsorption of As(III) on laterite soil. *J. Sep. Purif. Technol.* **2007**, *56*, 284–290. [CrossRef]
20. Maiti, A.; Thakur, B.K.; Basu, J.K.; De, S. Comparison of treated laterite as arsenic adsorbent from different locations and performance of best filter under field conditions. *J. Hazard. Mater.* **2013**, *262*, 1176–1186. [CrossRef]
21. Bakouan, C. Caractérisation de Quelques Sites Latéritiques du Burkina Faso: Application à L'élimination de L'arsenic (III) et (V) Dans Les Eaux Souterraines. Thèse de Doctorat en Cotutelle Entre l'Université Ouaga I Pr JKZ et de, l'Université de Mons en Belgique. 2018, pp. 1–241. Available online: <https://orbi.umons.ac.be/bitstream/20.500.12907/31806/1/Th%C3%A8se> (accessed on 1 February 2018).
22. Ouedraogo, R.D.; Bakouan, C.; Sorgho, B.; Guel, B. Caractérisation d'une latérite naturelle du Burkina Faso En Vue de l'élimination de l'arsenic (III) et l'arsenic (V) dans les eaux souterraines. *Int. J. Biol. Chem. Sci.* **2019**, *13*, 2959–2977. [CrossRef]
23. Nguyen, T.H.; Tran, N.H.; Vu, H.A.; Trinh, M.V.; Nguyen, T.V.; Loganathan, P.; Vigneswaran, S.; Nguyen, T.M.; Trinh, V.T.; Vu, D.L.; et al. Laterite as a low-cost adsorbent in a sustainable decentralized filtration system to remove arsenic from groundwater in Vietnam. *Sci. Total Environ.* **2020**, *699*, 134267. [CrossRef] [PubMed]
24. Nguyen, T.H.; Nguyen, A.T.; Loganathan, P.; Nguyen, T.V.; Vigneswaran, S.; Nguyen, T.H.H.; Nguyen, T.H. Low-Cost laterite-laden household filters for removing arsenic from groundwater in vietnam and waste management. *Process Saf. Environ. Prot.* **2021**, *152*, 154–163. [CrossRef]
25. Oladoja, N.A.; Ademoroti, C.M.A. The use of fortified soil-clay as on-site system for domestic wastewater purification. *Water Res.* **2006**, *40*, 613–620. [CrossRef]
26. Bonsor, H.C.; MacDonald, A.M.; Davies, J. Evidence for extreme variations in the permeability of laterite from a detailed analysis of well behaviour in Nigeria. *Hydrol. Process.* **2014**, *28*, 3563–3573. [CrossRef]
27. Bali, M. Influence de l'aération du massif filtrant sur les performances épuratoires du procédé d'infiltration-percolation. *Rev. Des. Sci. De L'eau* **2019**, *31*, 365–375. [CrossRef]
28. Centre Régional pour l'Eau Potable et l'Assainissement à Faible Coût (CREPA). La Déferrisation des eaux de forage: Synthèse des techniques expérimentées avec succès avec CREPA. Document Technique/CREPA. *Sticht. IRC Int. Water Sanit. Cent.* **1996**, *1*, 1–68.
29. Gul, A.; Hruza, J.; Yalcinkaya, F. Fouling and chemical cleaning of microfiltration membranes: A Mini-Review. *Polymers* **2021**, *13*, 846. [CrossRef] [PubMed]
30. Jeong, H.Y.; Jun, S.C.; Cheon, J.Y.; Minji, P. A review on clogging mechanisms and managements in aquifer storage and recovery (ASR) applications. *Geosci. J.* **2018**, *22*, 667–679. [CrossRef]
31. Wang, Y.; Liu, H.; Wang, S.; Li, X.; Wang, X.; Jia, Y. Simultaneous removal and oxidation of arsenic from water by δ -MnO₂ modify activate carbon. *J. Environ. Sci.* **2020**, *94*, 147–160. [CrossRef]
32. Nikié, J.; Agbaba, J.; Watson, M.A.; Tubié, A.; Šolić, M.; Maletić, S.; Dalmacija, B. Arsenic adsorption on Fe–Mn modified granular activated carbon (GAC–FeMn): Batch and fixed-bed column studies. *J. Environ. Sci. Health-Part. A Toxic/Hazard. Subst. Environ. Eng.* **2019**, *54*, 168–178. [CrossRef] [PubMed]
33. Meez, E.; Tolkou, A.K.; Giannakoudakis, D.A.; Katsoyiannis, I.A.; Kyzas, G.Z. Activated carbons for arsenic removal from natural waters and wastewaters: A Review. *Water* **2021**, *13*, 2982. [CrossRef]
34. Maazou, B.D.S.; Halidou, I.H.; Mousbahou, M.; Alma, M.; Adamou, Z. Elimination du chrome par du charbon actif élaboré et caractérisé à partir de la coque du noyau de Balanites Aegyptiaca élimination of the chromium by the élaborate activated coal and characterized from the cockle of the core of balanites aegyptiaca. *Int. J. Biol. Chem. Sci.* **2017**, *11*, 3050–3065. [CrossRef]

35. Essis, A.; Yao, Y.A.; Yao, K.U.; Albert, T. Optimisation de la préparation de charbons activés à base d'épis de maïs et caractérisation physico-chimique. *Int. J. Innov. Appl. Stud.* **2020**, *29*, 1161–1171.
36. Clotaire, M.; Avom, J.; Mpon, R. Evaluation des propriétés de charbons actifs de résidus de moabi (*baillonella toxisperma* pierre) par adsorption d'iode en solution aqueuse. *J. Water Sci.* **2019**, *29*, 51–60. [[CrossRef](#)]
37. Basu, M.; Guha, A.K.; Ray, L. Adsorption of lead on lentil husk in fixed bed column bioreactor. *Bioresour. Technol.* **2019**, *283*, 86–95. [[CrossRef](#)]
38. Ha, H.T.; Phong, P.T.; Minh, T.D. Synthesis of iron oxide nanoparticle functionalized activated carbon and its applications in arsenic adsorption. *J. Anal. Methods Chem.* **2021**, *2021*, 6668490. [[CrossRef](#)]
39. Kundu, S.; Gupta, A.K. Analyse et modélisation du fonctionnement des colonnes à lit fixe sur l'élimination de l'As(V) par adsorption sur du ciment revêtu d'oxyde de fer (IOCC). *J. Colloid. Interface Sci.* **2005**, *290*, 52–60. [[CrossRef](#)]
40. Sruthi, P.; Reddy, P. Effect of Alkali Concentration on swelling characteristics of transformed kaolinitic. *Clays Clay Miner.* **2020**, *68*, 373–393. [[CrossRef](#)]
41. Nguyen, T.A.H.; Ngo, H.H.H.; Guo, W.S.; Nguyen, T.T.; Vu, N.D.; Soda, S.; Nguyen, T.H.H.; Nguyen, M.K.; Tran, T.V.H.; Dang, T.T.; et al. White hard clam (*Meretrix lyrata*) shells as novel filter media to augment the phosphorus removal from wastewater. *Sci. Total Environ.* **2020**, *741*, 140483. [[CrossRef](#)]
42. Tran, H.N.; You, S.-J.; Chao, H.-P. Activated carbons from golden shower upon different chemical activation methods: Synthesis and characterizations. *J. Adsorpt. Sci. Technol.* **2017**, *36*, 95–113. [[CrossRef](#)]
43. Boakye, P.; Tran, H.N.; Lee, D.S.; Woo, S.H. Effect of water washing pretreatment on property and adsorption capacity of macroalgae-derived biochar. *J. Environ. Manag.* **2019**, *233*, 165–174. [[CrossRef](#)] [[PubMed](#)]
44. Mahatheva, K.; Loganathan, P.; Vinh, T.; Nur, T. Iron-Impregnated granular activated carbon for arsenic removal: Application to practical column filters. *J. Environ. Man.* **2019**, *239*, 235–243.
45. Vieira, W.T.; Bispo, M.D.; Farias, S.d.M.; Almeida, A.d.S.V.d.; da Silva, T.L.; Vieira, M.G.A.; Soletti, J.I.; Balliano, T.L. Activated carbon from macauba endocarp (*Acrocomia aculeate*) for removal of atrazine: Experimental and theoretical investigation using descriptors based on DFT. *J. Environ. Chem. Eng.* **2021**, *9*, 105–155. [[CrossRef](#)]
46. Rawat, S.; Maiti, A. A hybrid ultrafiltration membrane process using a low-cost laterite based adsorbent for efficient arsenic removal. *Chemosphere* **2023**, *316*, 1376–1385. [[CrossRef](#)]
47. Kalenda, G.M. Comportement des sols latéritiques compactés dans les remblais et digues de retenue des rejets miniers du Katanga (RDC). Thèse de Doctorat à l'Université Catholique de Louvain, Ottignies-Louvain-la-Neuve, Belgium, 2014; p. 275.
48. Podder, M.S.; Majumder, C.B. Fixed-Bed column study for As(III) and As(V) removal and recovery by bacterial cells immobilized on sawdust/MnFe₂O₄ Composite. *Biochem. Eng. J.* **2016**, *105*, 114–135. [[CrossRef](#)]
49. Carneiro, M.A.; Pintor, A.M.A.; Boaventura, R.A.R.; Botelho, C.M.S. Efficient removal of arsenic from aqueous solution by continuous adsorption onto iron-coated cork granulates. *Sustainability* **2022**, *432*, 128657. [[CrossRef](#)]
50. Pantić, K.; Bajić, Z.J.; Veličković, Z.S.; Nešić, J.Z.; Đolić, M.B.; Tomić, N.Z.; Marinković, A.D. Arsenic removal by copper-impregnated natural mineral tufa part II: A kinetics and column adsorption study. *Environ. Sci. Pollut. Res.* **2019**, *26*, 24143–24161. [[CrossRef](#)]
51. Goel, J.; Kadirvelu, K.; Rajagopal, C.; Kumar, V. Removal of lead (II) by adsorption using treated granular activated carbon: Batch and column studies. *J. Hazard. Mater.* **2005**, *125*, 211–220. [[CrossRef](#)]
52. Vijayasri, K.; Tiwari, A.; Chaudhari, C.V. Fixed-bed column studies on removal of As(V) by radiation grafted polymer 'Chitosan-g-MAETC. *Anal. Chem. Lett.* **2019**, *9*, 486–503. [[CrossRef](#)]
53. Bretzler, A.; Nikiema, J.; Lalanne, F.; Hoffmann, L.; Biswakarma, J.; Siebenaller, L.; Demange, D.; Schirmer, M.; Hug, S.J. Arsenic removal with zero-valent iron filters in Burkina Faso: Field and laboratory insights. *Sci. Total Environ.* **2020**, *737*, 39–66. [[CrossRef](#)] [[PubMed](#)]
54. Verma, L.; Singh, J. Removal of As(III) and As(V) from aqueous solution using engineered biochar: Batch and fixed-bed column study. *Int. J. Environ. Sci. Technol.* **2023**, *20*, 1961–1980. [[CrossRef](#)]
55. Nguyen, H.T.; Paripurnanda, S.R.; Kandasamy, L.J.; Nguyen, T.V.; Vigneswaran, S. Arsenic adsorption by low-cost laterite column: Longterm experiments and dynamic column modeling. *Process Saf. Environ. Prot.* **2022**, *160*, 868–875. [[CrossRef](#)]
56. Zhang, Y.; Xiong, L.; Xiu, Y.; Huang, K. Defluoridation in fixed-bed column filled with Zr(IV)-loaded garlic peel. *Microchem. J.* **2018**, *145*, 476–485. [[CrossRef](#)]
57. Maji, K.S.; Pal, A.; Pal, T. Arsenic removal from real-life groundwater by adsorption on laterite soil. *J. Hazard. Mater.* **2008**, *151*, 811–820. [[CrossRef](#)] [[PubMed](#)]
58. Maiti, A.; DasGupta, S.; Basu, J.K.; De, S. Adsorption of arsenite using natural laterite as adsorbent. *Sep. Purif. Technol.* **2007**, *55*, 350–359. [[CrossRef](#)]
59. Maji, S.K.; Kao, Y.-H.; Wang, C.-J.; Lu, G.-S.; Wu, J.-J.; Liu, C.-W. Fixed bed adsorption of As(III) on iron-oxide-coated natural rock (IOCNR) and application to real arsenic-bearing groundwater. *Chem. Eng. J.* **2012**, *203*, 285–293. [[CrossRef](#)]

Disclaimer/Publisher's Note: The statements, opinions and data contained in all publications are solely those of the individual author(s) and contributor(s) and not of MDPI and/or the editor(s). MDPI and/or the editor(s) disclaim responsibility for any injury to people or property resulting from any ideas, methods, instructions or products referred to in the content.